IEEE Access

Date of publication xxxx 00, 0000, date of current version xxxx 00, 0000.

*Digital Object Identifier 10.1109/ACCESS.2017.Doi Number*

# Stochastic Optimal Power Flow Integrating with Renewable Energy Resources and V2G Uncertainty Considering Time-Varying Demand: Hybrid GTO-MRFO Algorithm

**Mohamed H. Hassan[1], Ehab Mahmoud Mohamed [2*], Salah Kamel[3], Sid Ahmed El Mehdi Ardjoun[4]**

[1]Ministry of Electricity and Renewable Energy, Cairo, Egypt.
[2]Department of Electrical Engineering, College of Engineering in Wadi Addawasir, Prince Sattam Bin Abdulaziz University, Wadi Addawasir 11991, Saudi Arabia.
[3]Department of Electrical Engineering, Faculty of Engineering, Aswan University, Aswan 81542, Egypt.
[4]IRECOM Laboratory, Faculty of Electrical Engineering, Djillali Liabes University, Sidi Bel-Abbes 22000, Algeria.
Corresponding author: Ehab Mahmoud Mohamed (e-mail: ehab_mahmoud@aswu.edu.eg).

Acknowledgement: This project is sponsored by Prince Sattam bin Abdulaziz University (PSAU) as part of funding for its SDG Roadmap Research Funding Program project number PSAU-2023-SDG-16.

**ABSTRACT** Over the past ten years, global electricity networks have undergone rapid advancements, primarily driven by the widespread adoption of renewable energy resources (RES). While these sources have accompanied in a gathering of advantages, such as cost-effective operation of wind and solar photovoltaic (PV) installations and the mitigation of environmental hazards linked with traditional power sources, they have also introduced a host of challenges to planning and operation of power systems. Also, Plug-in electric vehicles (PEVs) stand out as a highly promising technology for reducing carbon emissions in the transportation sector, aligning with the global Net-zero target. The standard optimal power flow (OPF) problem, which is naturally nonlinear, has become even more complex with the addition of renewable energy sources and plug-in electric vehicles along with traditional thermal power generators. This increased complexity comes from the unpredictable and intermittent nature of these new resources. Monte Carlo techniques are used to estimate the production costs of renewable energy sources and plug-in electric vehicles (PEVs) and analyze their viability. The uncertainty of the renewable sources and PEVs is modeled using Weibull, lognormal, and normal probability distribution functions (PDFs). The comprehensive OPF, incorporating renewable energy components and PEVs, is cast as a single objective problem encompassing various objectives, such as decreasing fuel costs, total emissions, voltage deviations, and real transmission losses. This research shares a common objective by introducing a novel hybrid metaheuristic optimization algorithm (MRGTO) to address the OPF challenge. Additionally, the study explores the impact of renewable energy resources and Vehicle-to-Grid (V2G) on the stochastic OPF problem. The MRGTO employs artificial gorilla troops optimizer (GTO) with manta ray foraging optimization (MRFO) algorithm to achieve the optimal results for the OPF problem with stochastic RES and V2G. The developed technique is expected to increase the solution accuracy through increasing the solution diversity through an optimization procedure. Initial assessments are executed on benchmark functions. After that, a combined model of wind and PV-integrated IEEE 30-bus system are executed by the proposed MRGTO algorithm and other well-known optimization algorithms. Additionally, the effectiveness of the proposed method is assessed using the IEEE 30-bus test system under different scenarios. The evaluations have shown the proposed MRGTO technique to be superior at attainment a best solution for the OPF problem considering stochastic wind and PV power and V2G. Moreover, the obtained solutions confirmed the MRGTO technique would be more effective in optimization with quicker convergence rate, and higher convergence precision. After testing, the effectiveness of the MRGTO algorithm has been found to be much robust than the conventional artificial gorilla troops optimizer, manta ray foraging optimization, and other well-known published heuristics, metaheuristics, and hybrid optimization techniques.

**INDEX TERMS** Optimal Power Flow, plug-in electric vehicle, renewable energy sources, V2G, artificial gorilla troops optimizer, manta ray foraging optimization.

## I. INTRODUCTION

The demanding requirement to decrease operating costs in conventional power generators and reduce emissions of greenhouse gas from these types of generating units has encouraged many electric power firms to shift in the direction of utilize from the RES. Furthermore, developments in renewable energy technologies have greatly contributed to their rise as the most cost-effective and globally aware resources [1]. Photovoltaic (PV) and wind-turbine (WT) systems are among the RESs that have been integrated into power systems to reduce the negative environmental impact of fossil fuels [2]. However, the integration of RESs in the grid causes a significant challenge because of the unpredictability of wind speed and solar irradiation, which can lead to uncertainty [3][4]. To enhance the precision and practicality of wind and SPV modeling, the Weibull probability distribution function has been employed for the prediction of the wind speed [5], while the lognormal probability distribution function has been utilized to imitate the sporadic characteristics of solar irradiance in previous studies [6].

Presently, as an essential design plan of power-generating systems operation infrastructure in smart cities environment, electric vehicles (EVs) have concerned significant interest because of fossil fuel scarcity, wide environmental changes, and the rapid development of communication technology in smart cities [7]. The existence of electric vehicles introduces additional uncertainty, further complicating matters. Consequently, it is crucial to consider the dynamic nature of RESs to confirm the safe and profitable operation of the power system. The integration of RESs in smart grids has several advantages, such as reducing peak energy demand and lowering energy losses. However, because these RESs depend on weather conditions, uncertainty in weather forecasts can impact grid reliability and increase energy generation costs [8], [9]. Additionally, the integration of RESs in smart grids presents environmental and policy-related challenges [10].

The recent increasing rate of energy storage solutions, notably electric vehicles (EVs), featuring diverse charging profiles, has significantly impacted the optimization of power dispatch strategies. This trend has spurred a remarkable surge in research and publications within this domain [11]. One of the pivotal aspects of this evolution is the incorporation of EVs into the grid as mobile energy storage units. These PEVs not only serve as a means of transportation but also function as distributed energy resources [12]. They can both draw power from the grid and supply excess energy back to it, making them dynamic assets in the electricity system. The intersection of PEVs, wind, and PV systems in the power dispatch problem represents a complex and dynamic landscape. Researchers are actively exploring innovative approaches to optimize the utilization of these resources, taking into account the dynamic charging patterns of PEVs and the intermittent nature of wind and PV generation.

The OPF is a way used to regulate the best operating point in terms of control variables to improve choosy objective functions and has become a critical feature of the generation and operation of modern power systems [13] [14]. As RESs are being combined into the generation mix, they must be included in the OPF analysis [15]. However, the integration of PEVs into the electrical network poses a challenge due to their uncertain power consumption or injection behavior. PEVs' charging can increase the transmission lines' load, which can be addressed through the vehicle-to-grid (V2G) model. This model enables PEVs to supply surplus power to the grid through designated devices when stationary, thus mitigating the effect of their combined impact on the system [16].

Over the last ten years, the majority of research efforts have gone toward finding solutions for OPF problems related to thermal plants. Researchers' interest in the OPF problem combined with RESs has lately grown as a result of RESs' increased integration into the electricity system. Biswas et al. [17] try to find a best solution for the OPF problem using adopting various evolutionary techniques whereas considering the high penetration of thermal, wind, solar, and hydropower plants. Gaussian Bare-bones Levy Circulatory System-Based Optimization algorithm has been used to optimize OPF considering the WTs and PVs in [18]. In Ref. [19], a gradient bald eagle search optimization algorithm with local escaping operator method was suggested and assessed on the IEEE 30-bus power network integrated with renewable energy and V2G uncertainty. He et al. proposed a method for combined scheduling of wind, thermal, and hydropower, which includes spinning reserve [20]. When it comes to real-time economic dispatch (ED), precise prediction can lead to a narrower range of uncertainty than in long-term scheduling. In order to model the uncertain behavior of renewable generation plants and PEVs, probability distribution functions (PDFs) can be utilized, as demonstrated by Chang, who employed Weibull PDF for modeling wind speed and lognormal distribution for modeling solar irradiance [16]. Vaderobli et al. enhanced the energy cost for PV stations under various weather conditions [21], while the authors in [22] developed a hybrid optimization approach for short-term scheduling of solar-wind-hydrothermal generation. Hassan et al. [23] handle adopting a Chaotic Bonobo Optimizer (CBO) for solving three contradictive objective functions in which least fuel cost's values, emission level, and power loss are achieved. The modified white shark optimization has been utilized for reaching to the optimum results for the OPF issue [24], in which several kinds of renewable energies were incorporated.

The previous literature shows that instant OPFs have been utilized in the past. However, practical power systems are dynamic, and their operating conditions continuously

change. Therefore, decisions based solely on instant OPFs may not be accurate, which is why this paper employs a dynamic OPF that considers various time instances to provide system operators with correct and optimal solutions [25]. The main objective of this article is to reduce the total fuel cost, which includes the cost of conventional generators, the cost of RESs, and the generation cost for PEVs at different time intervals. To represent uncertainties related to wind, PV, and PEV systems, this study employs Weibull, lognormal, and normal probability density functions (PDFs), and uncertainty costs are computed by Monte Carlo simulations. Though, there are various uncertainties that need to be considered, and multiple methods can be used to calculate uncertainty costs. For example, in [26], the authors proposed a stochastic optimization process that accounts for uncertainties in electricity demand, natural gas infrastructures, PV generating units, and wind power generation by mixed-integer linear programming (MILP).

Also, according to the literature, employing metaheuristic algorithms as innovative methodologies for OPF problem involving Wind, PV, and EVs has demonstrated commendable outcomes. Although these algorithms have gained widespread approval, their performance metrics, encompassing factors such as convergence and efficiency, may exhibit notable disparities. Furthermore, the tenets of the no-free-lunch theorems underscore a fundamental reality: the absence of a universally superior metaheuristic algorithm capable of optimally addressing every conceivable optimization problem [27]. In light of this principle, the development of alternative, novel Metaheuristic Algorithms (MAs) holds the potential to yield superior outcomes compared to those documented in the existing literature. Thus, the dynamic landscape of metaheuristic approaches prompts a search for newer methodologies that could possibly cover the achievements of their already published counterparts. These reasons encourage us to propose a novel optimization technique.

The Artificial Gorilla Troops Optimizer (GTO) and the Manta Ray Foraging Optimization (MRFO) algorithm represent two robust population-based metaheuristic techniques. They draw inspiration from the social intelligence observed in gorilla troops and the distinct foraging strategies of manta rays, including chain foraging, cyclone foraging, and somersault foraging. Those techniques, similar other optimization methods, start with a randomly produced group of solutions inside the area of the problem [28]. After this, these solutions are updated using information from previous solutions and historical data and, but only for a limited number of repeats [29]. As the solutions slowly improve, their quality gets better, helping find more ideal answers for the problem. These techniques were used in many different areas and thoroughly tested with lots of test functions, with good results. However, they have some weaknesses. For example, they are too slow to converge for some complex, high-dimensional problems, and they cannot guarantee finding the absolute best solution quickly enough.

The GTO method has the advantages of fast convergence and high effectiveness. Furthermore, GTO is defined by its straightforwardness, easy application, and fast convergence, but it can still get stuck in local optima [30]. In the literature, some articles have been done in order to address these restrictions. In [31], the authors suggested a new technique for regulating the strength control parameters of the GTO using fitness-based crossover (FBC) strategy and periodic Tangent Flight (TF) operator to improve the exploration and exploitation capabilities of the technique to address parameters extraction of three different PV modules. In [32], the authors suggested a hybrid GTO and zebra optimization approach in order to progress the stochastic behavior of the GTO technique for Hybrid optimized-ANFIS based MPPT for hybrid microgrid. In this article, hybrid metaheuristic optimization technique (MRGTO) is suggested for addressing and optimizing the OPF problem with incorporated RES and PEVs. This improvement of MRGTO method rises exploration capability compared to the GTO and MRFO algorithms. Additionally, the investigation of the MRGTO method will not diminish as the number of iterations increases, avoiding it from being stuck in local minimum values. The MRGTO algorithm is confirmed when it is applied on the enhanced IEEE 30-bus power system with EVs and RESs and obtained results are compared to several optimization algorithms. The IEEE 30-bus test systems have been adapted through incorporating wind, solar, and EVs power systems. Although the standard OPF is already a large-scale, nonlinear, non-convex constrained optimization issue, the complexity increases further when integrating Wind, PV, and PEVs due to the intermittent nature of these sources. Also, this paper focus on the dynamic OPF while the load demand is varying in order to show the effect of the high penetration of RES beside the V2G station on the operational flexibility of the electric power system. Figure 1 shows the proposed framework.

The main contributions of this article can be outlined as follows:

- Presenting MRGTO, an enhanced version of Artificial gorilla troops optimizer (GTO) based on hybrid with manta ray foraging optimization (MRFO) to show improved performance in real-world optimization problems, primarily in OPF situations, taking into consideration the complexity of stochastic RESs and EVs.
- Comparing the competences and attained results of the proposed technique and its counterparts including beluga whale optimization (BWO), runge kutta algorithm (RUN), tuna swarm optimization (TSO), and dung beetles optimizer (DBO), as well as the original GTO and MRFO techniques, displays the suggested MRGTO's optimization power.

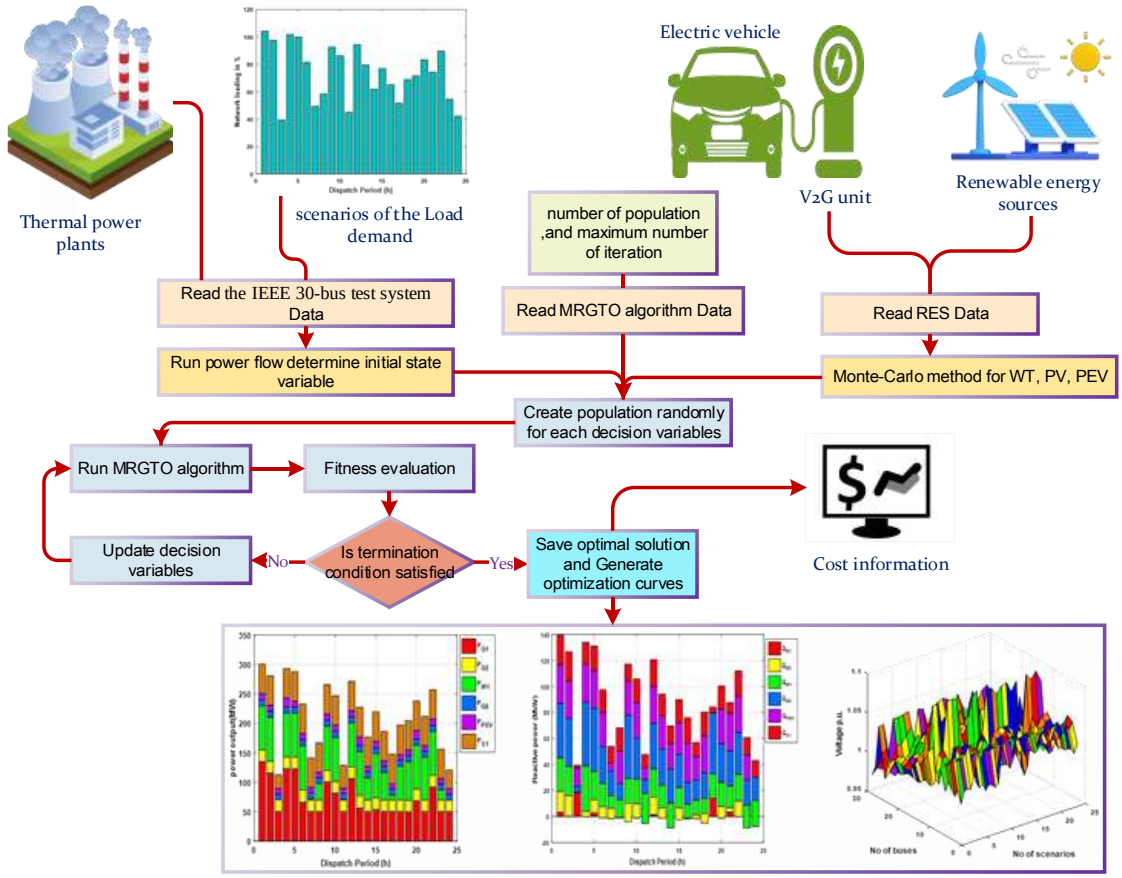


**FIGURE 1.** **Configuration of the proposed framework**

- Approving the presented MRGTO for improving the different OPF functions and reduction of operating cost and emission level. The results demonstrate that MRGTO can attain a high performance in solving the different OPF issues.
- Emphasis on dynamic OPF considerations, specifically addressing varying load demand to showcase the influence of high-RES penetration and Vehicle-to-Grid (V2G) stations on electric power system operational flexibility.

The rest of the paper is organized as follows: Section 2 outlines the mathematical formulation of OPF and its operating constraints, and Sections 3 explains the output models for WT, SPV, EVs units and load demand uncertainty. Section 4 introduces the original GTO algorithm and the MRFO algorithm, while Section 5 applies the MRGTO algorithm to solve the OPF problem in the presence of RESs and EVs, presenting the results obtained for seven benchmark functions. Section 6 presents statistical analysis and robustness, and Section 7 concludes the paper by summarizing the main findings.

## II. The OPF's Calculated Model

The dynamic optimal power flow (DOPF) problem is a complex and nonlinear one, which requires identifying the most appropriate control variable values that minimize the fitness function while satisfying several operational constraints. The primary goal of this paper is to reduce the total operation cost, including the expenses related with thermal and RESs, in addition to the cost of integrating EVs into the network. The control variables optimized in this study include real and reactive power outputs of generators, besides voltages, transformer tap ratios, and shunt VAR capacitors [33]. In this study, our overarching objective is to tackle this complexity head-on and devise strategies that lead to a more efficient and cost-effective power system. Specifically, we aim to optimize the allocation of resources by curbing the total generation cost. This encompasses a multifaceted approach, encompassing the optimal utilization of both traditional thermal generation and increasingly vital renewable energy sources. Moreover, with the rising prominence of electric vehicles (EVs) as an integral part of the modern energy landscape, we are also dedicated to addressing the challenges of integrating these EVs into the

power grid, while minimizing the associated costs and enhancing grid reliability.

The underlying objective of the DOPF is to find the optimal values of control variables that achieve specific goals while adhering to a set of equality and inequality constraints. Mathematically, the OPF problem can be formulated as follows:

$$Minimize, f(x,u) \tag{1}$$

Constrained by:

$$g(x,y) = 0 \tag{2}$$

$$h(x,y) \leq 0 \tag{3}$$

### A. The Operation Cost for the Thermal generating units

The fossil fuel-powered thermal generators' function, and the expense of the fuel can be articulated in the subsequent way [13]:

$$F(P_{cg}) = \sum_{i=1}^{N_g} \alpha_i P_{cg,i}^2 + \beta_i P_{cg,i} + \gamma_i \tag{4}$$

where $F$ represents the fuel cost for thermal power plants, $N_g$ refers to the whole number of the traditional generators, $P_{cg,i}$ denotes the real power output from generator i. the coefficients of the operating cost according to the i-th thermal generators are represented by $\alpha_i$ , $\beta_i$ , and $\gamma_i$.When the multi-valve loading effect is taken into account, the quadratic fuel cost becomes more accurate. Thus, the cost function incorporating the valve point loading effect (VPLE) can be formulated as follows [13]:

$$F(P_{cg}) = \sum_{i=1}^{N_g} \alpha_i P_{cg,i}^2 + \beta_i P_{cg,i} + \gamma_i + \left| e_i \times \sin(g_i(P_{cg,i}^{min} - P_{cg,i})) \right| \tag{5}$$

The valve point cost coefficients of the i-th thermal generator are denoted by $e_i$ and $g_i$ while $P_{cg,i}^{min}$ denotes the lowest active power that the i-th generators can produce.

### B. The operating Cost for WT and SPV generators

Developing an accurate cost model for Renewable Energy Sources (RES), such as wind or solar, can be difficult due to their variable nature. In a study published in [34], the authors have proposed a cost model for RES that is owned by the ISO and does not include fuel costs. It is critical to assess the scheduled versus actual capacity of RES as it can affect the total operational cost of the power system. By precisely estimating the RES capacity, operation costs can be minimized. To construct the cost function for RES sources, two scenarios must be considered. Firstly, if the actual capacity is less than the scheduled capacity, the Independent System Operator (ISO) must compensate for the shortfall by dispatching power from other plants, incurring a reserve cost. Secondly, if the RES's real power exceeds its scheduled capacity, surplus power goes to waste unless conventional generators reduce their output. The ISO will have to pay a penalty cost equal to the excess quantity of RES if this is not possible.

Wind turbine (WT) and solar photovoltaic (SPV) units operate without requiring fuel and typically only incur main maintenance or operational costs. The energy produced by these renewable sources is charged based on a jointly contracted agreement. Private parties are responsible for bearing the direct costs of WT and SPV units, which can be defined as below:

$$C_{W_j}\left(P_{W_{s,j}}\right) = g_{W_d} P_{W_{s,j}} \tag{6}$$

The direct cost of the j-th wind turbine generator is represented by $C_{W_j}$, while $g_{W_d}$ refers to the WT generator's coefficient of direct cost. $P_{W_{s,j}}$ denotes the scheduled production of the j-th wind generator. The following formula is used to calculate the scheduled power related with the k-th SPV generator's direct cost:

$$C_{S_k}(P_{S_{s,k}}) = g_{S_d} P_{S_{s,k}} \tag{7}$$

where the scheduled generation of the k-th SPV unit is indicated by $P_{S_{s,k}}$, and the SPV unit's direct cost coefficient is represented by $g_{S_d}$.

### C. Cost Calculation of the WT generating Units

The equation below represents the penalty cost that system operators bear for the surplus power produced using WT units:

$$\begin{aligned} C_{U_{w,j}}\left(P_{W_{a,j}} - P_{W_{s,j}}\right) &= p_{W,j}\left(P_{W_{a,j}} - P_{W_{s,j}}\right) \\ &= p_{W,j}\int_{P_{W_{s,j}}}^{P_{W_{r,j}}} \left(P_{W,j} - P_{W_{s,j}}\right) F_W(P_{W,j})\, dP_{W,j} \end{aligned} \tag{8}$$

where $P_{W_{a,j}}$ , and $P_{W_{s,j}}$, represent the available, schedule output power from j-th wind turbine generator, respectively and $P_{W_{r,j}}$ refers to the j-th WT unit's rated output power. $p_{W,j}$ denotes the coefficient of the penalty cost for the j-th wind turbine unit while $F_W(P_{W,j})$ refers to the PDF of the j-th WT generator's generated power. The following formula is used to determine reserve cost, which is the cost that is dependent on this power reserve.:

$$\begin{aligned} C_{O_{w,j}}\left(P_{W_{s,j}} - P_{W_{a,j}}\right) &= R_{W,j}\left(P_{W_{s,j}} - P_{W_{a,j}}\right) \\ &= R_{W,j}\int_{0}^{P_{W_{s,j}}} \left(P_{W_{s,j}} - P_{W_{a,j}}\right) F_W(P_{W,j})\, dP_{W,j} \end{aligned} \tag{9}$$

The coefficient for the reserve cost by the j-th WT generating unit is represented by $R_{W,j}$. Moreover, the calculation of the probability of power production for multiple WT generators at different wind velocities.

### D. Cost Calculation of SPV Units

The following formula can be used to determine the penalty cost for the k-th SPV unit:

$$C_{U_{S,K}}\left(P_{S_{a,K}} - P_{S_{s,K}}\right) = p_{S,K}\left(P_{S_{a,K}} - P_{S_{s,K}}\right) = p_{S,K} \cdot F_S\left(P_{S_{a,K}} > P_{S_{s,K}}\right) \cdot \left[E\left(P_{S_{a,K}} > P_{S_{s,K}}\right) - P_{S_{s,K}}\right] \quad (10)$$

$P_{S_{a,K}}$ *and* $P_{S_{s,j}}$ represent the K-th SPV generator's current and scheduled power, respectively, $p_{S,K}$ denotes the coefficient of the penalty cost with respect to the K-th SPV generators, $F_S\left(P_{S_{a,K}} > P_{S_{s,K}}\right)$ indicates the possibility that the k-th SPV generators will produce surplus power compared to $P_{S_{a,K}}$. $E\left(P_{S_{a,K}} > P_{S_{s,K}}\right)$ refers to the expected excess electricity output. The reserve cost is computed using the following formula in the event that it is overestimated:

$$C_{O_{S,K}}\left(P_{S_{s,K}} - P_{S_{a,K}}\right) = R_{S,K}\left(P_{S_{s,K}} - P_{S_{a,K}}\right) = R_{S,K} \cdot F_S\left(P_{S_{a,K}} < P_{S_{s,K}}\right) \cdot \left[P_{S_{s,K}} - E\left(P_{S_{a,K}} < P_{S_{s,K}}\right)\right] \quad (11)$$

where $R_{S,K}$ refers to the coefficient of reserve cost for the K-th SPV generator, $F_S\left(P_{S_{a,K}} < P_{S_{s,K}}\right)$ denotes the absence of SPV generators' potential, and $E\left(P_{S_{a,K}} < P_{S_{s,K}}\right)$ represents the SPV generator's predictable power fewer than $P_{S_{s,K}}$.

### E. Cost of EV units

The use of V2G technology presents a unique opportunity for intelligent energy management and electricity trade. With renewable energy sources becoming increasingly prevalent, V2G provides utility companies with the ability to utilize the energy stored in electric vehicles to mitigate grid congestion and meet peak load demands. V2G technology allows electric vehicles to function as mobile storage assets, optimizing energy usage and supporting the grid, while still allowing EV owners to control when their vehicle is available for use [35]. As well as researching the development and suitability of electric vehicles (EVs) and battery-electric vehicles (BEV), attention must also be given to the growing symbiotic relationship between the developing smart grid and electric vehicles. Currently, several car manufacturers are investing significant resources in producing and developing new electric vehicle models. The formula for determining the direct cost of the n-th EV unit in relation to scheduled power is as below:

$$C_{ev_n}\left(P_{ev_{s,n}}\right) = d_{ev_n} P_{ev_{s,n}} \quad (12)$$

In this equation, $d_{ev_n}$ is the the n-th EV generator's direct cost coefficient. $P_{ev_{s,n}}$ represents the scheduled production using the n-th EV generator.

The n-th EV unit's reserve cost is expressed as follows:

$$C_{R_{ev,n}}\left(P_{ev_{s,n}} - P_{ev_{av,n}}\right) = H_{Rev,n}\left(P_{ev_{s,n}} - P_{evav,n}\right) = H_{Rev,n}\int_0^{P_{pev,n}} \left(P_{ev_{s,n}} - P_{ev,n}\right) f_{ev}(p_{ev,n})\, dp_{ev,n} \quad (13)$$

where $P_{ev_{s,n}}$ and $P_{ev_{av,n}}$ represent the n-th EV unit's actual and scheduled power, respectively, $H_{Rev,n}$ represents the reserve cost coefficient for the n-th electric vehicle generators. The reserve cost is computed using the following formula in the event that it is overstated:

$$C_{P_{pev,n}}\left(P_{ev_{s,n}} - P_{ev_{av,n}}\right) = H_{Pev,n}\left(P_{ev_{av,n}} - P_{evs,n}\right) = H_{Pev,n}\int_{P_{ev,n}}^{P_{evr,n}} \left(P_{ev,n} - P_{evs,n}\right) f_{ev}(p_{ev,n})\, dp_{ev,n} \quad (14)$$

where $P_{evr,n}$ represents the n-th EV unit's rated power. $H_{Pev,n}$ denotes the penalty cost coefficient for the n-th electric vehicle generators.

### F. Carbon Tax Model

Conventional units release harmful pollutants into the surroundings, and with the escalation of production from thermal units, the discharge of gases. These dangerous emissions are computed as follows:

$$E = \sum_{i=1}^{N_G} \left(a_i P_{cg,i}^2 + b_i P_{cg,i} + c_i\right) \times 0.01 + \omega_i e^{\left(P_{cg,i}\,\mu_i\right)} \quad (15)$$

where $a_i$ , $b_i$ , $c_i$ , $\omega_i$ *and* $\mu_i$ represent the thermal generators' emission coefficients.

Recently, several countries have implemented carbon taxes as a measure to safeguard the environment, encourage the adoption of RESs, and address the risks of global warming. Power generation firms are under significant pressure to generate green energy from sustainable sources and limit their detrimental emissions. Consequently, carbon taxes are being imposed on such polluting models. The cost of carbon emissions, expressed in dollars per hour, is given by:

$$C_{EC} = C_T \times E \quad (16)$$

where $C_T$ refers to the carbon tax of gasses per unit value.

### G. Objective Functions

In this paper, we discuss the objective functions used for the DOPF problem, which are comprised of several models discussed in the previous subsections. Specifically, we consider two fitness functions, which are described below:

#### 1) REDUCING OF THE TOTAL COST

Without taking emissions into account, the first objective function suggested in this article is made in order to reduce the overall cost. The second fitness function, on the other hand, accounts for emissions. As a result, the first fitness function seeks to reduce the subsequent:

$$F_1 = F(P_{cg}) + \sum_{j=1}^{N_W}\Big[C_{W_j}\left(P_{W_{s,j}}\right) + C_{U_{w,j}}\left(P_{W_{a,j}} - P_{W_{s,j}}\right) + C_{O_{w,j}}\left(P_{W_{s,j}} - P_{W_{a,j}}\right)\Big] + \sum_{K=1}^{N_P}\Big[C_{S_k}\left(P_{S_{s,k}}\right) + C_{U_{S,K}}\left(P_{S_{a,K}} - P_{S_{s,K}}\right) + C_{O_{S,K}}\left(P_{S_{s,K}} - P_{S_{a,K}}\right)\Big] + \sum_{l=1}^{N_V}\Big[C_{ev_l}\left(P_{ev_{s,l}}\right) + C_{U_{ev,l}}\left(P_{ev_{a,l}} - P_{ev_{s,l}}\right) + C_{O_{ev,l}}\left(P_{ev_{s,l}} - P_{ev_{a,l}}\right)\Big] \quad (17)$$

where $N_W, N_P$ *and* $N_V$ refer to the combined count of WT, SPV, and EV generators, respectively. When considering the modeling of CT, the second objective function can be obtained by adding the CT from Equation 16 to Equation 17.

$$F_2 = F(P_{cg}) + \sum_{j=1}^{N_W}\Big[C_{W_j}\left(P_{W_{s,j}}\right) + C_{U_{w,j}}\left(P_{W_{a,j}} - P_{W_{s,j}}\right) + C_{O_{w,j}}\left(P_{W_{s,j}} - P_{W_{a,j}}\right)\Big] + \sum_{K=1}^{N_P}\Big[C_{S_k}\left(P_{S_{s,k}}\right) + C_{U_{S,K}}\left(P_{S_{a,K}} - P_{S_{s,K}}\right) + C_{O_{S,K}}\left(P_{S_{s,K}} - P_{S_{a,K}}\right)\Big] + \sum_{l=1}^{N_V}\Big[C_{ev_l}\left(P_{ev_{s,l}}\right) + C_{U_{ev,l}}\left(P_{ev_{a,l}} - P_{ev_{s,l}}\right) + C_{O_{ev,l}}\left(P_{ev_{s,l}} - P_{ev_{a,l}}\right)\Big] + C_{EC} \quad (18)$$

Furthermore, it should be noted that these two objective functions are subject to certain equality and inequality constraints, which can be expressed as shown below:

### 2) THE ACTIVE POWER LOSSES

This equation can be used to define the active power losses:

$$P_L = \sum_{k=1}^{n_l} G_k[V_i^2 + V_j^2 - 2V_iV_jcos(\theta_i - \theta_j)] \quad (19)$$

where $P_L$ denotes the active power loss, $G_k$ refers to the $k$'th line's conductance. $V_i, V_j$, $\theta_i$ and $\theta_j$ are the voltage magnitudes at buses i and j and their angles, respectively.

### 3) THE VOLTAGE DEVIATIONS

The following formula can be used to express the voltage fluctuations at the load buses:

$$V_D = \sum_{j=1}^{N_L} |V_k - 1| \quad (20)$$

One per unit (p.u.) is the reference value for a nominal value that can be used as a benchmark. $N_L$ shows the bus number relating to the load.

### 4) EQUALITY RESTRICTIONS

The equality constraints, which may be expressed as follows, represent the power flow equations that are used to preserve power equilibrium:

$$P_{Gi} - P_{Di} - V_i\sum_{j=1}^{N_L} V_j(G_{ij}\cos\theta_{ij} + B_{ij}\sin\theta_{ij}) = 0 \quad (21)$$

$$Q_{Gi} - Q_{Di} - V_i\sum_{j=1}^{N_L} V_j(G_{ij}\sin\theta_{ij} - B_{ij}\cos\theta_{ij}) = 0 \quad (22)$$

where the actual and reactive power generated are, respectively, $P_{Gi}$ and, $Q_{Gi}$. While, $P_{Di}$ and, $Q_{Di}$ reflect the bus j's demand active and reactive power, respectively. $G_{ij}$ denotes the transfer conductance between two buses, and $B_{ij}$ denotes their susceptance.

### 5) INEQUALITY RESTRICTIONS

The constraints on inequality are related to the operational limitations that are placed on the various components of the power system, including the security limitations that are depending on the lines and load busses.

### 6) UNIT RESTRICTIONS

All producing buses must have their real power and voltage limits kept within predetermined lower and upper bounds.

$$V_{Gi}^{min} \le V_{Gi} \le V_{Gi}^{max}, \quad i = 1,2,3\ldots,N_T \quad (23)$$

$$P_{cg,i}^{min} \le P_{cg,i} \le P_{cg,i}^{max}, \quad i = 1,2,3\ldots,N_g \quad (24)$$

$$P_{W_{s,j}}^{min} \le P_{W_{s,j}} \le P_{W_{s,j}}^{max}, \quad j = 1,2,3\ldots,N_W \quad (25)$$

$$P_{S_{s,K}}^{min} \le P_{S_{s,K}} \le P_{S_{s,K}}^{max}, \quad k = 1,2,3\ldots,N_P \quad (26)$$

$$P_{PEV_{PEV,l}}^{min} \le P_{PEV_{PEV,l}} \le P_{PEV_{PEV,l}}^{max}, \quad l = 1,2,3\ldots,N_V \quad (27)$$

$$Q_{cg,i}^{min} \le Q_{cg,i} \le Q_{cg,i}^{max}, \quad i = 1,2,3\ldots,N_g \quad (28)$$

$$Q_{W_{s,j}}^{min} \le Q_{W_{s,j}} \le Q_{W_{s,j}}^{max}, \quad j = 1,2,3\ldots,N_W \quad (29)$$

$$Q_{S_{s,K}}^{min} \le Q_{S_{s,K}} \le Q_{S_{s,K}}^{max}, \quad k = 1,2,3\ldots,N_P \quad (30)$$

$$Q_{PEV_{PEV,l}}^{min} \le Q_{PEV_{PEV,l}} \le Q_{PEV_{PEV,l}}^{max}, \quad k = 1,2,3\ldots,N_V \quad (31)$$

where $N_T$ represents the quantity of unit buses. The voltage limits for these buses are specified in Equation 23, while Equations 24 through 27 establish the limits on active power output for thermal units, wind turbines (WT), solar photovoltaic (SPV), and EV units. Additionally, Equations 28 through 21 describe the reactive power capacities of the producing buses.

### 7) LIMITATIONS ON LINE AND LOAD BUS VOLTAGES

$$S_{li} \le S_{li}^{max}, \quad i = 1,2,3\ldots,N_l \quad (32)$$

$$V_{Li}^{min} \le V_{Li} \le V_{Li}^{max}, \quad i = 1,2,3\ldots,N_L \quad (33)$$

where, $S_{li}$ denotes the apparent power of the line i'th. $S_{li}^{max}$ signifies the extreme border of the apparent power of line i'th. $V_{Li}^{min}$ , $V_{Li}^{max}$ indicate the minor and higher voltage magnitude, respectively. $N_l$ refers to the number of transmission lines.

## III. The Stochastic WT power, SPV Power, EV power Models, and Load demand uncertainty

### A. Modelling of wind turbine power

In order to represent the average power production of WT units, Weibull PDFs are employed in the subsequent manner [36]:

$$f_v(v)=\frac{K}{C}\cdot\left(\frac{v}{C}\right)^{K-1}.e^{-\left(\frac{v}{C}\right)^{K}} \tag{34}$$

where ν represents the wind speed m/s, K refers to Weibull distribution shape parameter, and C indicates the Weibull distribution scale parameter.

Where K stands for the Weibull distribution shape parameter, C for the Weibull distribution scale parameter, and v for the wind speed in meters per second.

The following represents the Weibull distribution mean:

$$M_{wt}=C\cdot\Gamma\left(1+{}^{1}/_{K}\right) \tag{35}$$

The gamma function formula is as follows:

$$\Gamma x=\int_{0}^{\infty} t^{x-1}e^{-t}\,dt \quad , x>0 \tag{36}$$

The power output of wind turbine (WT) units is primarily affected by wind speed and the power curve of the WT, which can be described by the following equation:

$$P_w(v)=\begin{cases} 0 & v\le v_{ci} \;\&\; v>v_{co} \\ \dfrac{v^2-v_{ci}^2}{v_{nom}^2-v_{ci}^2}\cdot P_{W_r} & v_{ci}<v\le v_{nom} \\ P_{W_r} & v_{nom}<v\le v_{co} \end{cases} \tag{37}$$

where $v_{ci}$ , $v_{co}$ , and $v_{nom}$ are the cut-in, cut-out and rated wind speed, respectively. Whereas, WT units' rated power is represented by $P_{W_r}$. It is clear from Eq. (37), that there is no output power if v rises over $v_{co}$ and falls below $v_{ci}$. Moreover, power is produced by the wind turbine while the wind speed is between two values $v_{nom}$ and $v_{co}$. For those distinct regions, possibilities can be stated as follows [37]:

$$F_w(P_w)\{P_w=0\}=1-\exp\left(-\left(\frac{v_{ci}}{C}\right)^{k}\right)+\exp\left(-\left(\frac{v_{co}}{C}\right)^{k}\right) \tag{38}$$

$$F_w(P_w)\{P_w=P_{wr}\}=\exp\left(-\left(\frac{v_{nom}}{C}\right)^{k}\right)-\exp\left(-\left(\frac{v_{co}}{C}\right)^{k}\right) \tag{39}$$

Unlike the discrete regions mentioned earlier, the power output of wind turbines (WT) is continuous between the cut-in and rated wind speeds. Therefore, the potential for this range is determined as follows [24]:

$$F_w(P_w)=\frac{K(v_{nom}-v_{ci})}{C^K*P_{wr}}\left(v_{ci}+\frac{P_w}{P_{wr}}(v_{nom}-v_{ci})\right)^{k-1}*\exp\left(-\left(\frac{v_{ci}+\frac{P_w}{P_{wr}}(v_{nom}-v_{ci})}{c}\right)^{k}\right) \tag{40}$$

### B. Modelling of Solar Photovoltaic power

A lognormal function is used to more precisely characterize the frequency distribution in order to account for changing weather conditions. The parameters for the lognormal distribution function are calculated using the global irradiation mean and standard deviation. A lognormal Probability Density Function (PDF) governs sun irradiance (I), which affects the output of solar photovoltaic (SPV) devices. The following formula [38] can be used to express the likelihood of the solar irradiance:

$$f_I(I)=\frac{I}{I\mu\sqrt{2\pi}}\cdot e^{\left(\frac{-[\ln X-\sigma]^2}{2\mu}\right)}, \quad I>0 \tag{41}$$

where the standard deviation (STD) and mean are denoted, respectively, by $\mu$ and $\sigma$. The following formula can be used to express the lognormal distribution's mean:

$$M_{ld}=e^{\left(\sigma+\frac{\mu^2}{2}\right)} \tag{42}$$

The relationship between the solar irradiance and the energy produced by the solar photovoltaic (SPV) units can be stated directly as follows [39].

$$P_{sr}(I)=\begin{cases} P_{sr}\left(\dfrac{I^2}{I_{sr}I_c}\right) & ;\ 0<I<I_c \\ P_{sr}\left(\dfrac{I}{I_{sr}}\right) & ;\ I>I_c \end{cases} \tag{43}$$

In the given equation, $P_{sr}$ denotes the SPV units' rated output, $I_c$ is a specific irradiance point, and $I_{sr}$ refers to the solar irradiance at the rated environment. It is crucial to remember that the energy allocated for solar power is negotiable and is decided upon by the private company selling the solar power as well as the system operators. The following computations can be used to calculate the costs related to overestimating or underestimating the output of the solar photovoltaic (SPV) devices [40]:

$$C_{U_S}(P_{S_a}-P_{S_s})=p_S(P_{S_a}-P_{S_s})=p_S\sum_{N=1}^{N+}[P_{S_{S+}}-P_{S_S}]*f_{ps+} \tag{44}$$

$$C_{O_S}(P_{S_s}-P_{S_a})=R_S(P_{S_s}-P_{S_a})=R_S\sum_{N=1}^{N-}[P_{S_S}-P_{S_{S-}}]*f_{ps-} \tag{45}$$

where $P_{S_{S+}}$ and $P_{S_{S-}}$ denote the excess power and insufficient power. $f_{ps+}$ and $f_{ps-}$ indicate the relative occurrences of $P_{S_{S+}}$ and $P_{S_{S-}}$.

### C. Modelling of vehicle-to-grid power

As stated in reference [41], the distribution of the deployment of electric vehicles as a vehicle-to-grid (V2G) source follows a normal distribution and can be mathematically represented by:

$$f_{pev} = \frac{1}{\sqrt{2\pi\varphi^2}} e^{-\frac{(P_{pev}-\mu)^2}{2\varphi^2}} \quad (46)$$

where $\mu$ and $\varphi$ are the mean and SD of a normal PDF. $P_{pev}$ refers to the available V2G power.

### D. Modelling of Load demand uncertainty

Uncertainties in load modeling are represented using the PDF of a normal distribution, as follows:

$$f_d(P_d) = \frac{1}{\sigma_d\sqrt{2\pi}} exp\left[-\frac{(P_d-\mu_d)^2}{2{\sigma_d}^2}\right] \quad (47)$$

In this equation, $\mu_d$ and $\sigma_d$ denote the average and std values, respectively. $P_d$ refers to the probability density of the load's normal distribution. The scenarios of the Load demand were generated through Monte Carlo simulations using a normal distribution PDF with a sample size of 1000, where $\mu_d$ is equal to 70 and $\sigma_d$ is equal to 10, as displayed in Figure 2. The probability of load demand and the scenario of predictable load can be calculated as follows:

$$\tau_{d,i} = \int_{P_{d,i}^{min}}^{P_{d,i}^{max}} \frac{1}{\sigma_d\sqrt{2\pi}} exp\left[-\frac{(P_d-\mu_d)^2}{2{\sigma_d}^2}\right] dP_d \quad (48)$$

$$P_{d,i} = \frac{1}{\tau_{d,i}} \int_{P_{d,i}^{min}}^{P_{d,i}^{max}} \frac{P_d}{\sigma_d\sqrt{2\pi}} exp\left[-\frac{(P_d-\mu_d)^2}{2{\sigma_d}^2}\right] dP_d \quad (49)$$

where, $P_{d,i}^{min}, P_{d,i}^{max}$ are the max and min bounds of interval $i$. The backward reduction algorithm (BRA), as detailed in reference [6], was utilized for the purpose of scenario reduction.

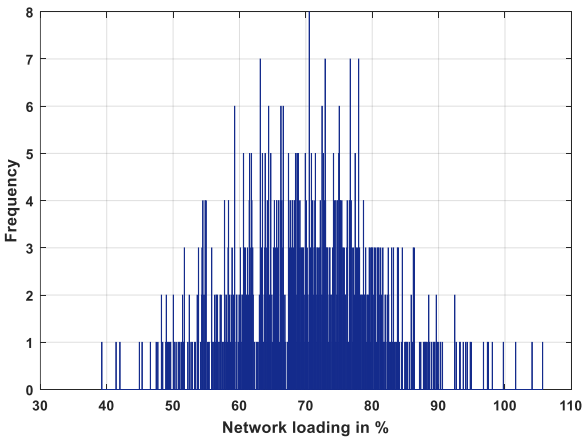


**FIGURE 2. scenarios of the Load demand through Monte Carlo simulations.**

## IV. Mathematical model of the metaheuristic Algorithms

This study introduces an innovative approach to improve the performance of the artificial gorilla troops optimizer (GTO) algorithm by hybridizing it with manta ray foraging optimization (MRFO). The objective is to address the identified weaknesses of the GTO while retaining its existing search operators. The proposed method involves replacing a portion of the worst solutions generated in each iteration with solution candidates according to the representative candidates of the current population. Through incorporating this MRFO algorithm in the GTO, the balance between exploration and exploitation is improved, and the algorithm's ability to handle premature convergence is enhanced, resulting in significant optimization performance improvements. The authors suggest that other algorithms with similar shortcomings could also benefit from the proposed MRFO technique. The initial steps of the original GTO and MRFO algorithms are described in this section.

### A. Gorilla Troops Optimizer (GTO)

#### 1) EXPLORATION PHASE

During the exploration stage, three different operators were employed: To investigate the GTO algorithm further, relocate to an unidentified area. The shift to other gorillas, the second component, improves the balance between exploitation and exploration. The 3rd component relates to the exploration stage; specifically, moving to a well-known region knowingly improves the GTO algorithm's capacity to find various improvement spaces. The following equation can be used to represent these various operators [42]:

$$GX(t+1) = \begin{cases} (ub-lb)\times r_1 + lb, & rand < z \\ (r_2 - C)\times X_r(t) + D\times B, & rand \geq 0.5 \\ X(i) - D\times\left(D\times\left(X(t)-GX_r(t)\right) + r_3\times\left(X(t)-GX_r(t)\right)\right), & rand < 0.5 \end{cases}$$

$$C = (\cos(2\times r_4)+1)\times\left(1-\frac{it}{Maxit}\right) \quad (50)$$

$$D = C\times k$$
$$B = E\times X(t)$$
$$E = [-C, C]$$

Where, $GX(t+1)$ refers to the gorilla candidate location in the following cycle. $lb$ and $ub$ represents the lower and upper limits of the variables, respectively. $r_1$, $rand$, $r_2$, $r_3$, and $r_4$ indicate random values ranging from 0 to 1. $z$ is a variable with a range of 0 to 1. $X(t)$ is the present vector of the gorilla location whereas $X_r(t)$ represents one among the gorillas chosen at random from the entire group of gorillas and also $GX_r(t)$. $k$ denotes a random number between -1 and 1.

#### 1) EXPLOITATION STAGE

There are two behaviors used during the exploitation stage. In the exploitation phase, two tactics are utilized. When $C \geq W$, the first tactic is called "Follow the Silverback." The parameter $W$ needs to be set prior to the optimization process. Mathematically, the first tactic is determined as below:

$$GX(t+1) = D \times M \times (X(t) - X_{silverback}) + X(t)$$
$$M = \left( \left| \frac{1}{N} \sum_{i=1}^{N} GX_i(t) \right|^{g} \right)^{\frac{1}{g}} \quad (51)$$
$$g = 2^{D}$$

Where $X_{silverback}$ indicates the optimal solution, $N$ represents the maximum number of gorillas.

The second step is the struggle for adult females, and it is used once $C < W$. The equation that follows is used to compute this mechanism:

$$GX(i) = X_{silverback} - (X_{silverback} \times Q - X(t) \times Q) \times A$$
$$Q = 2 \times r_5 - 1 \quad (52)$$
$$A = \beta \times H$$
$$H = \begin{cases} N_1, & rand \geq 0.5 \\ N_2, & rand < 0.5 \end{cases}$$

Where $\beta$ indicates a parameter that needs to be set to a value prior to optimization. $r_5$ refers to a value chosen at random between 0 and 1.

### B. Manta Ray Foraging Optimization (MRFO)

Manta Ray Foraging Optimization (MRFO) suggested by Zhao et al. in 2020 [43]. It imitates the behavior of a manta ray. The creation of MRFO involves mimicking common foraging techniques like chaining, cyclone, and somersaulting. Manta rays observe the position of the plankton and then swim towards it, establishing an organized line so that the plankton that the preceding manta rays missed will be consumed by the subsequent manta rays. The location with a larger concentration of plankton is preferable. With the exception of the initial one, all manta rays now travel in the direction of the best position as well as the one in front of it. This process, referred to as "chain foraging," has the following mathematical expression [44]:

$$X_{i,j}(t+1) = \begin{cases} X_{i,j}(t) + \left(X_{best,j}(t) - X_{i,j}(t)\right) \times (r(:) - \lambda)\Delta\forall_i = 1, j \in N_{Var} \\ X_{i,j}(t) + \left(X_{i-1,j}(t) - X_{i,j}(t)\right) \times (r(:) - \lambda)\Delta\forall_i > 1 : N_{pop} \end{cases} \quad (53)$$

$$\varphi = 2 \times r(:) \times \sqrt{\left|\log\left(r(:)\right)\right|} \quad (54)$$

When a group of manta rays locates a large concentration of plankton in deep water, they join together head-to-tail to form a spiral chain. Each manta ray in the chain goes in the direction of the plankton position and the one in front of it. This process, referred to as "cyclone foraging," can be stated as follows:

$$X_{i,j}(t+1) = \begin{cases} X_{best,j}(t) + \Delta X_{i,j} \times (r - \beta)\Delta\forall_i = 1, j \in N_{Var} \\ X_{best,j}(t) + r \times \left(x_{i-1,j}(t) - X_{i,j}(t)\right) + \beta \times \Delta X_{i,j}\Delta\forall_i > 1 : N_{pop} \end{cases} \quad (55)$$

$$\beta = 2 \times exp\left(r_1 \times \frac{T_{max} - t + 1}{T_{max}}\right) \times \sin(2\pi r_1) \quad (56)$$

In order to maximize plankton intake, manta rays move in a frequent, unpredictable, cyclic, and local manner during the final stage of "somersault foraging." Every manta ray moves to and from the plankton position, which serves as a reference, before somersaulting to a new location. This step has the following mathematical expression:

$$X_{i,j}(t+1) = X_{i,j}(t) + SF \times \left(r_2 X_{best,j} - r_3 X_{i,j}(t)\right)\Delta\forall_i \in N_{pop} \quad (57)$$

$X_{best,j}$ can be well-defined as shown in Eq. (54) which describes the optimum position with high food concentration. If the low concentration is confirmed, the random location is set as shown in Eq. (57).

$$X_{i,j}(t+1) = \begin{cases} X_{best,j}(t) + \Delta X_{i,j} \times (r - \beta)\Delta\forall_i = 1, j \in N_{Var} \\ X_{best,j}(t) + r \times \left(x_{i-1,j}(t) - X_{i,j}(t)\right) + \beta \times \Delta X_{i,j}\Delta\forall_i > 1 : N_{pop} \end{cases} \quad (58)$$

$$\beta = 2 \times exp\left(r_1 \times \frac{T_{max} - t + 1}{T_{max}}\right) \times \sin(2\pi r_1) \quad (59)$$

$$X_{i,j}(t+1) = \begin{cases} X_{rand}(t) + \Delta X_{i,j} \times (r - \beta)\Delta\forall_i = 1, j \in N_{Var} \\ X_{best,j}(t) + r \times \left(x_{i-1,j}(t) - X_{i,j}(t)\right) + \beta \times \Delta X_{i,j}\Delta\forall_i > 1 : N_{pop} \end{cases} \quad (60)$$

$$X_{rand}(:) = Lb + r(:) \times (Hb - Lb) \quad (61)$$

Actually, there are two distinct characteristics that metaheuristic algorithms share: exploitation and exploration. Metaheuristic algorithms are superior to other algorithms because of these two traits. Within MRFO, search spaces will be conducted if $t/T_{max}$ is less than rand. The MRFO control system is described by $N_{pop}$, $T_{max}$, and $SF$ which should be closely adhered to guarantee its optimal performance.

### C. Hybrid GTO and MRFO algorithm (MRGTO)

The flowchart of the MRGTO technique is shown in Figure 3, where the position of the MRFO in the hybrid algorithm is highlighted. By incorporating the MRFO, the MRGTO algorithm is able to explore more extensively, leading to an enhanced performance. The basic steps of the proposed MRGTO technique can be outlined by the iterative steps displayed in Algorithm 1.

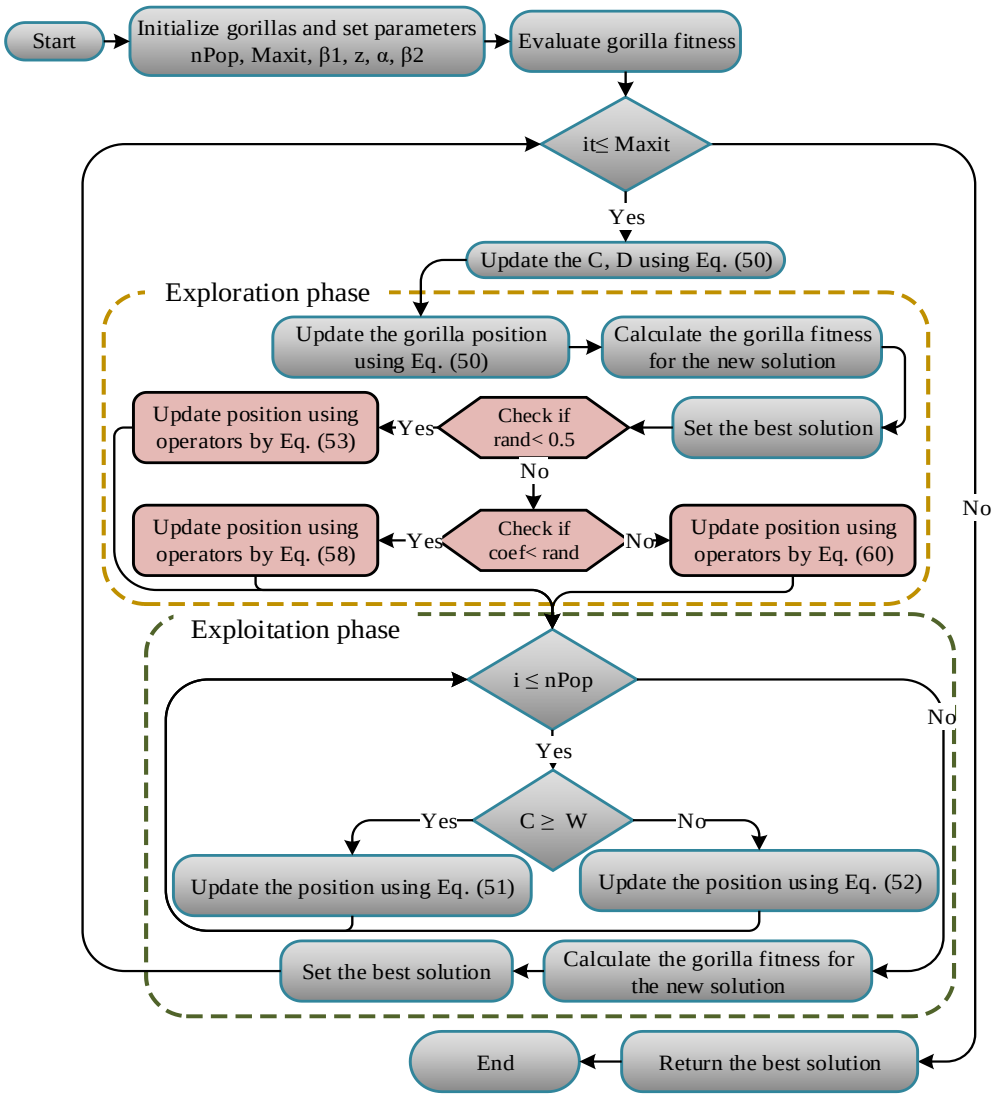


**FIGURE 3.** **Flowchart of proposed MRGTO algorithm.**

**Algorithm 1**: Pseudocode of the MRGTO technique

*Set the control parameter (problem dimension (d), maximum number of iterations, population size), lower and upper limits (lb, ub)*
*Set the population's initial value at random.*
*Assess the objective function of the new solution*
*Determine the optimal outcome.*
***While*** *iter* ≤ *MaxIt*
*Update the C and D using Eq. (50)*
% Exploration phase
***For*** *i=1:N*
*Update the location Gorilla using Equation (50)*
***End For***
% Create group
*Calculate the objective function values of Gorilla*
*if GX is better than X, replace them*
*Set Xsilverback as the location of silverback (best location)*
***For*** *i=1:N*
***If*** $rand < 0.5$

```
% Chain foraging
            Update the new position of each individual by Eq. (55)
          Else If
            If coef < rand
% Spiral foraging
                Update the new position of each individual by Eq. (58)
            Else If
%Somersault foraging
                Update the new position of the each individual using Eq.(60)
          End If
        End If
      End For
% Exploitation phase
      For i=1:N
        If |C| ≥ 1
          Update the place of Gorilla by Equation (51)
        Else If
          Update the place of Gorilla by Equation (52)
        End If
      End For
% Create group
    Verify the new positions' boundaries and evaluate the fitness values.
    Choose the new solution if the fitness improves
    iter=iter+1
  End while
 Output the optimal solution
```

### D. Computational complexity

The GTO technique's computational complexity depends on three essential procedures: initialization, objective function evaluation, and updating of gorillas. Since there is N gorilla, the computational complexity in the initialization procedure is equal to O(N). In contrast, the computational complexity in the update mechanism procedure is according to two stages of exploration and exploitation. In each of the stages, an updating operation is executed on all the solutions in the optimization area, and the optimal solution is performed, which is equal to O(T × N) + O(T × N × D) × 2. Where T indicates the maximum value of iterations, and D refers to the dimensions of the issues. Consequently, the GTO technique's computational complexity is O(N × (1 + T + TD) × 2). When the computational complexity of the MRFO's part is added, The exploration phase increased by O(T × N × D). Consequently, the MRGTO algorithm's computational complexity is O(N × (1 + T + TD) × 3).

## V. Simulation Results and Discussion

The results of the experiments conducted on 7 common test functions using the suggested technique and modern methods are shown in this section. Ref. [45] provides the mathematical formulation for these benchmark functions. The experiments provide a comprehensive evaluation of the techniques. Additionally, the section includes four examples that assess the effectiveness and applicability of the previously described MRGTO method.

### A. Benchmark functions

In this subsection, a demonstration is presented to exhibit the exceptional performance of the MRGTO method by conducting experiments on 7 benchmark functions, implemented in MATLAB (R2016a) on a computer with an Intel(R) Core i5-4210U CPU 2.40 GHz and 8GB RAM. The experiments were carried out to compare the MRGTO algorithm with seven recently proposed techniques, namely MRFO, BWO, RUN, DBO, TSO, and the original GTO algorithm. The maximum number of iterations for all studied algorithms was 200, and the number of populations was 50. Table I displays the parameter settings of the studied techniques.

TABLE I
THE PARAMETER SETTINGS FOR THE ALGORITHMS USED IN THE COMPARATIVE STUDY.

| Algorithm | Parameter |
|---|---|
| MRGTO | $\beta = 3, W = 0.8, P = 0.03, S = 2$ (Default) |
| GTO | $\beta = 3, W = 0.8, P = 0.03$ (Default) |
| BWO | $W_f$ = [0.1 0.05] (Default) |
| MRFO | $S$=2 (Default) |
| DBO | $k, \lambda = 0.1, b = 0.3, S = 0.5$ (Default) |

The average value and standard deviation of the results achieved by these algorithms were utilized to evaluate their

performance. Lower average value and standard deviation indicate greater stability and robustness in global optimization competence. Table II displays the statistical outcomes attained using the MRGTO algorithm and 5 other well-known methods for solving the seven benchmark functions, where the best results are highlighted in boldface. According to the table, the MRGTO technique surpasses the other methods in terms of average value for most of the benchmark functions. The lowest average rank value in Figure 4 belongs to MRGTO, indicating its superior performance over all other algorithms. This result confirms the effectiveness of our approach in identifying global optima for various problems. Additionally, Figure 5 presents the convergence curves for each benchmark function, which demonstrate that the MRGTO approach has a significantly superior convergence characteristics compared to the MRFO, BWO, RUN, DBO, TSO, and the original GTO algorithm. The rapid convergence capability of the MRGTO approach enhances its possible as a competent approach for solving real-world optimization problems. In conclusion, the results prove that the MRGTO technique is highly efficient and operative for solving these types of problems. The MRFO and GTO algorithms also exhibit robust effectiveness and rank as the second and third best, respectively.

TABLE II

THE STATISTICAL RESULTS OF BENCHMARK FUNCTIONS BY THE MRGTO TECHNIQUE AND OTHER RECENT METHODS.

| Function | | MRGTO | GTO | MRFO | BWO | RUN | DBO | TSO |
|---|---|---|---|---|---|---|---|---|
| F1 | Best | 0 | 1.3E-176 | 8.8E-180 | 1.5E-111 | 9.07E-86 | 2.59E-64 | 4.6E-118 |
| | Mean | 0 | 9.1E-152 | 3E-168 | 3.8E-106 | 5.02E-77 | 4.6E-40 | 1.07E-94 |
| | Median | 0 | 4.2E-170 | 8.2E-174 | 6.8E-108 | 1.06E-82 | 2.24E-49 | 5.3E-106 |
| | Worst | 0 | 1.8E-150 | 5.3E-167 | 2.5E-105 | 1E-75 | 5.64E-39 | 2.15E-93 |
| | std | 0 | 4.1E-151 | 0 | 6.8E-106 | 2.24E-76 | 1.35E-39 | 4.8E-94 |
| | Rank | 1 | 3 | 2 | 4 | 6 | 7 | 5 |
| F2 | Best | 2.7E-199 | 2.96E-85 | 5.73E-92 | 1.95E-57 | 1.04E-47 | 6.66E-36 | 2.98E-58 |
| | Mean | 2.8E-187 | 1.44E-80 | 2.78E-85 | 2.56E-54 | 1.87E-43 | 2.95E-22 | 1.66E-50 |
| | Median | 5.6E-191 | 5.06E-82 | 8.8E-87 | 1.15E-54 | 1.2E-44 | 7.84E-30 | 2.01E-52 |
| | Worst | 5E-186 | 9.29E-80 | 3.19E-84 | 1.18E-53 | 2.3E-42 | 5.34E-21 | 2.41E-49 |
| | std | 0 | 2.93E-80 | 7.82E-85 | 3.58E-54 | 5.35E-43 | 1.19E-21 | 5.44E-50 |
| | Rank | 1 | 3 | 2 | 4 | 6 | 7 | 5 |
| F3 | Best | 0 | 3.8E-167 | 1.7E-172 | 6.4E-104 | 5.75E-77 | 7.93E-70 | 3.4E-113 |
| | Mean | 0 | 3.9E-149 | 5.2E-162 | 5.5E-100 | 2.33E-62 | 6.56E-18 | 1.48E-89 |
| | Median | 0 | 9.3E-157 | 4.9E-167 | 1.2E-101 | 1.5E-69 | 1.23E-43 | 9.2E-100 |
| | Worst | 0 | 7.4E-148 | 8.3E-161 | 7.3E-99 | 4.54E-61 | 1.31E-16 | 2.79E-88 |
| | std | 0 | 1.7E-148 | 1.8E-161 | 1.6E-99 | 1.01E-61 | 2.93E-17 | 6.24E-89 |
| | Rank | 1 | 3 | 2 | 4 | 6 | 7 | 5 |
| F4 | Best | 1.2E-196 | 8.11E-88 | 3.32E-88 | 9.97E-55 | 1.35E-42 | 1.13E-36 | 4.03E-60 |
| | Mean | 1.2E-186 | 1.3E-80 | 1.1E-83 | 2.03E-52 | 2.09E-35 | 1.11E-17 | 8.06E-49 |
| | Median | 2.2E-192 | 8.8E-83 | 1.57E-84 | 5.03E-53 | 5.61E-39 | 3.95E-26 | 1.61E-50 |
| | Worst | 2.3E-185 | 1.37E-79 | 1.44E-82 | 1.38E-51 | 4.16E-34 | 1.94E-16 | 8.05E-48 |
| | std | 0 | 3.51E-80 | 3.22E-83 | 4.03E-52 | 9.3E-35 | 4.35E-17 | 1.89E-48 |
| | Rank | 1 | 3 | 2 | 4 | 6 | 7 | 5 |
| F5 | Best | 1.13E-10 | 4.82E-05 | 24.05046 | 0.000406 | 23.34961 | 25.89342 | 3.3E-05 |
| | Mean | 4E-06 | 3.890629 | 24.74472 | 0.010977 | 24.73586 | 26.53501 | 2.932789 |
| | Median | 1.91E-06 | 0.003429 | 24.73866 | 0.006422 | 24.85999 | 26.54883 | 0.100044 |
| | Worst | 2.32E-05 | 26.5186 | 25.81043 | 0.05599 | 26.52757 | 27.55468 | 26.85013 |
| | std | 7.38E-06 | 9.448749 | 0.428115 | 0.015734 | 0.832917 | 0.385201 | 8.100797 |
| | Rank | 1 | 4 | 6 | 2 | 5 | 7 | 3 |
| F6 | Best | 1.25E-30 | 1.28E-07 | 4.8E-06 | 2.47E-08 | 7.23E-09 | 0.000529 | 5.72E-06 |
| | Mean | 9.27E-20 | 0.000152 | 2.36E-05 | 5.36E-07 | 1.19E-08 | 0.009263 | 0.003695 |
| | Median | 2.34E-24 | 2.01E-05 | 1.09E-05 | 3.77E-07 | 1.19E-08 | 0.005537 | 0.00104 |
| | Worst | 1.82E-18 | 0.001805 | 0.000139 | 1.4E-06 | 2.24E-08 | 0.03888 | 0.018609 |
| | std | 4.06E-19 | 0.0004 | 3.13E-05 | 4.28E-07 | 3.7E-09 | 0.009978 | 0.00494 |
| | Rank | 1 | 5 | 4 | 3 | 2 | 7 | 6 |
| F7 | Best | 6.29E-06 | 5.83E-06 | 1.75E-05 | 2.65E-06 | 3.74E-05 | 0.00037 | 2.22E-05 |
| | Mean | 9.16E-05 | 0.000168 | 0.000226 | 0.000257 | 0.00042 | 0.004664 | 0.000684 |
| | Median | 7.22E-05 | 0.000152 | 0.00019 | 0.000225 | 0.000413 | 0.004214 | 0.00065 |
| | Worst | 0.000237 | 0.000421 | 0.000832 | 0.000674 | 0.000865 | 0.012705 | 0.002054 |
| | std | 7.58E-05 | 0.00012 | 0.000189 | 0.000205 | 0.000268 | 0.003369 | 0.000585 |
| | Rank | 1 | 2 | 3 | 4 | 5 | 7 | 6 |
| Average Rank | | 1 | 3.285714 | 3 | 3.571429 | 5.142857 | 7 | 5 |
| Final ranking | | 1 | 3 | 2 | 4 | 6 | 7 | 5 |

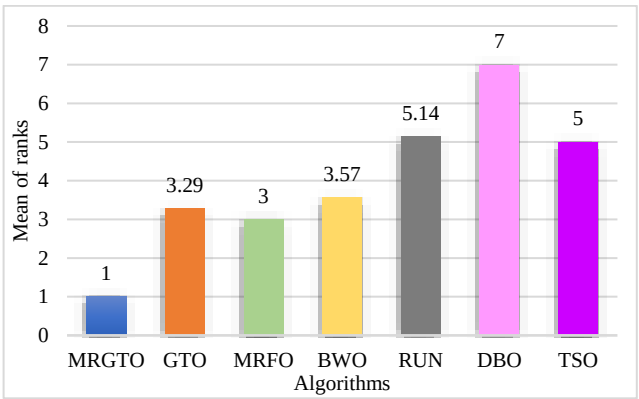


**FIGURE 4.** **The average ranks attained using the tied rank test for 23 functions using several techniques.**

**Statistical Analysis of MRGTO:** Table III demonstrates the statistical analysis of discrepancies between MRGTO and other algorithms by the Wilcoxon rank-sum test (WRST), a paired examination for identifying significant differences between two approaches. The symbols "+/=/-" in the table show whether MRGTO performs better, similarly, or worse than the comparison approach at a significance level of α=0.05. The table also presents the statistical results of MRGTO in several dimensions and functions, representing its comparative performance compared to the comparison method. The results expose that MRGTO outperforms other comparison methods in the statistics of these benchmark functions Therefore, it can be concluded that the MRGTO method shows superior performance compared to other approaches across most functions, highlighting its substantial benefit over other techniques.

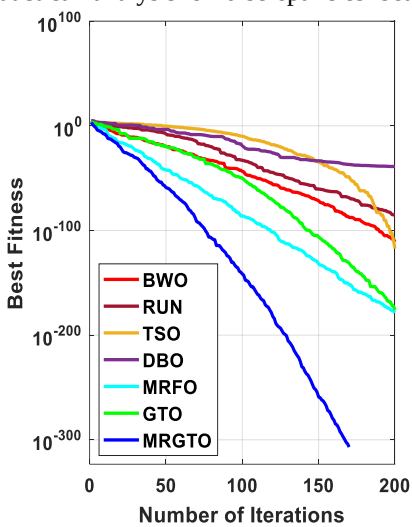


F1

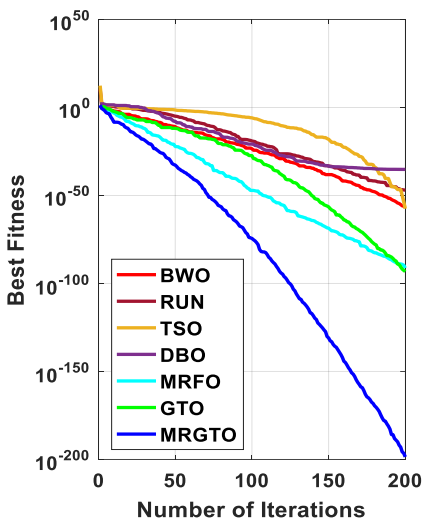


F2

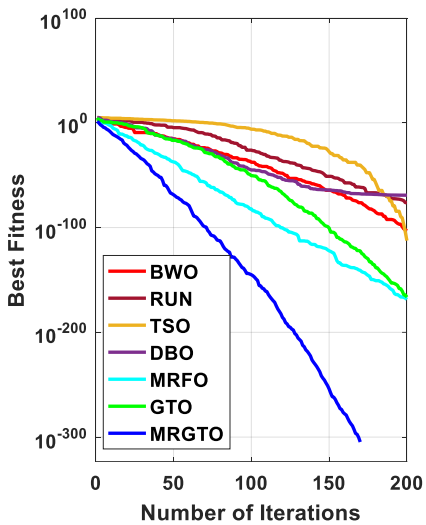


F3

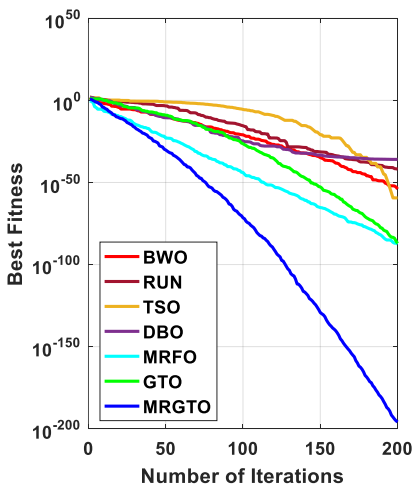


F4

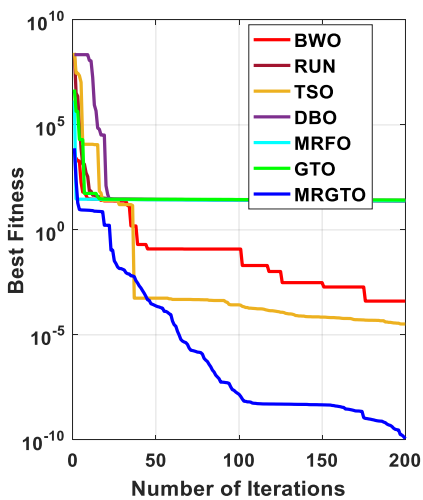


F5

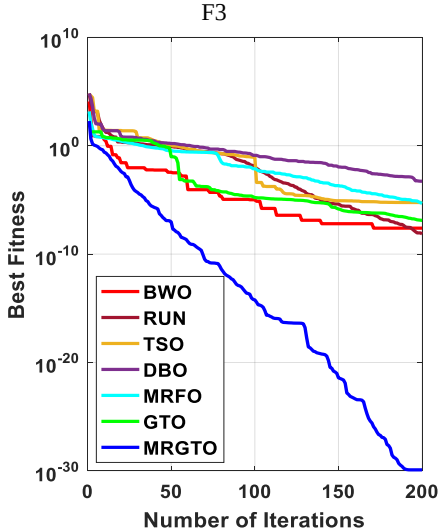


F6

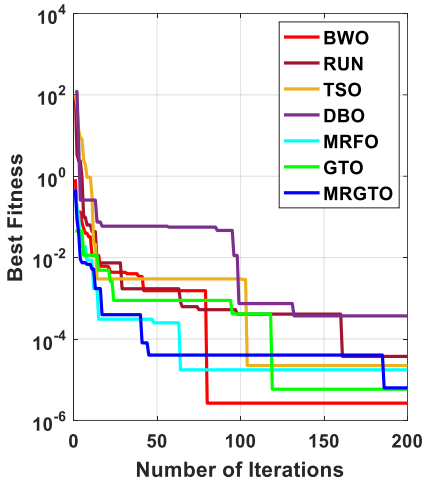


**FIGURE 5.** **The convergence curves of the studied techniques for seven benchmark functions.**

TABLE III
THE STATISTICAL RESULTS ATTAINED BY THE WILCOXON RANK-SUM TEST.

| MRGTO vs. | GTO | | MRFO | | DBO | | TSO | | RUN | | BWO | |
|---|---|---|---|---|---|---|---|---|---|---|---|---|
| Function | P | winner | P | winner | P | winner | P | winner | P | winner | P | winner |
| F1 | 8.01E-09 | + | 8.01E-09 | + | 8.01E-09 | + | 8.01E-09 | + | 8.01E-09 | + | 8.01E-09 | + |
| F2 | 6.80E-08 | + | 6.80E-08 | + | 6.80E-08 | + | 6.80E-08 | + | 6.80E-08 | + | 6.80E-08 | + |
| F3 | 8.01E-09 | + | 8.01E-09 | + | 8.01E-09 | + | 8.01E-09 | + | 8.01E-09 | + | 8.01E-09 | + |
| F4 | 6.80E-08 | + | 6.80E-08 | + | 6.80E-08 | + | 6.80E-08 | + | 6.80E-08 | + | 6.80E-08 | + |
| F5 | 6.27E-08 | + | 6.27E-08 | + | 6.27E-08 | + | 6.27E-08 | + | 6.27E-08 | + | 6.27E-08 | + |
| F6 | 6.80E-08 | + | 7.90E-08 | + | 6.80E-08 | + | 6.80E-08 | + | 6.80E-08 | + | 6.80E-08 | + |
| F7 | 5.65E-02 | = | 1.56E-01 | = | 6.80E-08 | + | 1.61E-04 | + | 4.68E-05 | + | 4.70E-03 | + |
| WRST (+/=/-) | 6/1/0 | | 6/1/0 | | 7/0/0 | | 7/0/0 | | 7/0/0 | | 7/0/0 | |

## B. The study case results

This section assesses the MRGTO technique's performance using the modified IEEE-30 bus test system. The objective is to lower the overall cost of generation and accelerate the convergence of the OPF problem, which includes EVs and RESs. We examine four scenarios, both with and without the V2G energy source. On a laptop with an I7-8700 CPU and 16 GB RAM, MATLAB 2016a and MATPOWER are used to run the simulation. The algorithms are run ten times with a population of fifty and a 200-iteration on each run. The two traditional GTO and MRFO algorithms, along with other currently used techniques, are contrasted with the MRGTO algorithm. Two objective functions including generator cost and total cost with a carbon tax are the basis for the comparison. The outcomes demonstrate that, with regard to both objectives, the MRGTO algorithm performs better than the other optimization techniques.

Six generators and 24 load buses connected by 41 branches make up the IEEE 30-bus system. Bus 1 is the slack bus. According to [13], the range of voltage magnitudes for load buses and generators is 0.95 p.u. to 1.1 p.u.; for tap-changing transformers, it is 0.9 p.u. to 1.1 p.u.; and for VAR compensators, it is 0 p.u. to 0.05 p.u. In this study, the system is updated by adding electric vehicle (EV), wind turbine (WT), and solar photovoltaic (SPV) units in addition to the current thermal generators. The thermal generators are situated at buses 1, 2, and 8, and in case studies 1 and 2, there is also an SPV unit at bus 13, a WT unit at bus 5, and a bus 11 unit. For cases 3 and 4, the EV unit is located at bus 11 instead of the WT unit. Figure 6 illustrates the modified system grid, which includes three generators. All of the cost and emission coefficients that were employed in the thermal generators' estimates are shown in Table IV.

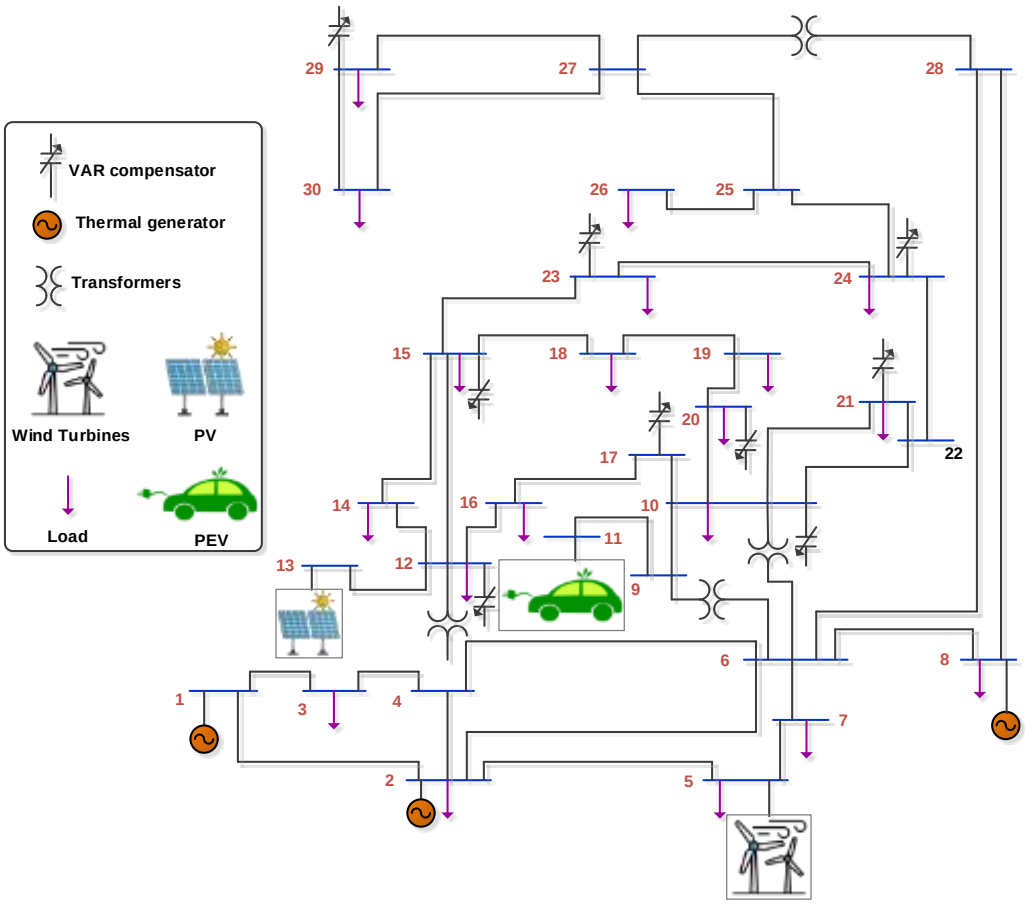


**FIGURE 6.** **The Modified IEEE 30-bus test system.**

TABLE IV
THERMAL GENERATORS' COSTS AND EMISSION COEFFICIENTS FOR THE SYSTEM UNDER INVESTIGATION.

| Unit | Bus no. | $\alpha$ | $\beta$ | $\gamma$ | $e$ | $g$ | $a$ | $b$ | $c$ | $\omega$ | $\mu$ |
|---|---|---|---|---|---|---|---|---|---|---|---|
| $P_{G1}$ | 1 | 0 | 2 | 0.00375 | 18 | 0.037 | 4.091 | -5.554 | 6.49 | 0.0002 | 6.667 |
| $P_{G2}$ | 2 | 0 | 1.75 | 0.0175 | 16 | 0.038 | 2.543 | -6.047 | 5.638 | 0.0005 | 3.333 |
| $P_{G8}$ | 8 | 0 | 3.25 | 0.00834 | 12 | 0.045 | 5.326 | -3.55 | 3.38 | 0.002 | 2 |

The frequency distribution of wind speeds for the WT generators using Weibull fitting is displayed in Figures 7a and 7b [46]. The power curve was derived after 8000 Monte-Carlo simulations. The WT generator at bus 5 has Weibull Probability Density Function (PDF) parameters of c = 9 and k = 2, whereas the WT generator at bus 11 has PDF parameters of c = 10 and k = 2. The Weibull distribution average for buses 5 and 11 is $M_{wt}$ = 7.976 m/s and 8.862 m/s, respectively. An installed 3 MW wind turbine had cut-in wind speed ($v_{ci}$= three m/s, cut-out wind speed ($v_{co}$ = twenty-five m/s), and rated wind speed ($v_{nom}$ = sixteen m/s).

The process for calculating the lognormal PDF parameters, which are based on the average and standard deviation (STD) of the global irradiation as stated in [47], is comparable to the procedure used to calculate the PV generators' output. In particular, the following criteria are chosen: = 6, = 0.6, and I = 483 W/m is the lognormal mean. The frequency distribution is then produced using the Monte-Carlo approach with a sample size of 8000, as seen in Fig. 8a, which is fitted to the lognormal distribution of solar irradiation. Additionally, Figure 8b shows the histogram for the SPV units' output, illustrating how the variability in solar irradiance causes the SPV output to be stochastic.

This article has been accepted for publication in IEEE Access. This is the author's version which has not been fully edited and content may change prior to final publication. Citation information: DOI 10.1109/ACCESS.2024.3425754



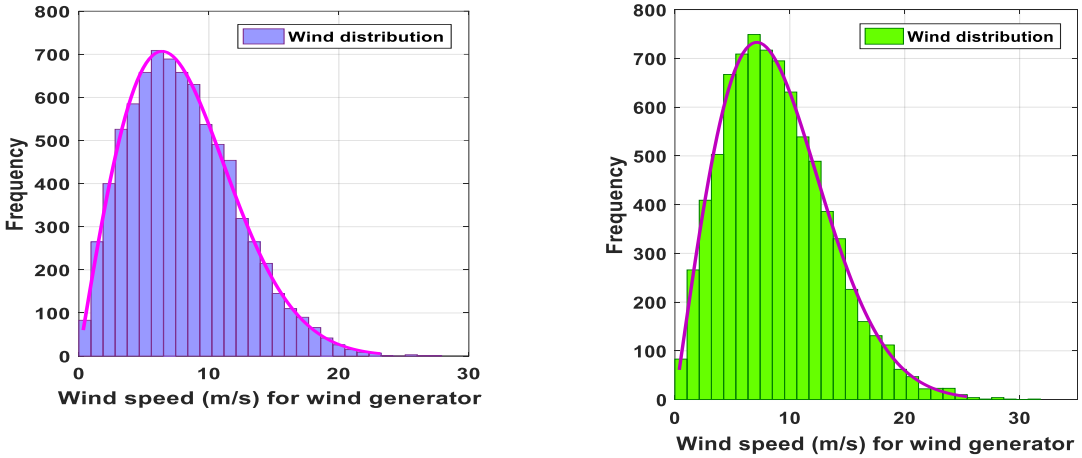


(a) at bus 5 (b) at bus 11

**FIGURE 7.** **The distribution of wind speed for the WT units located at bus 5 and 11.**

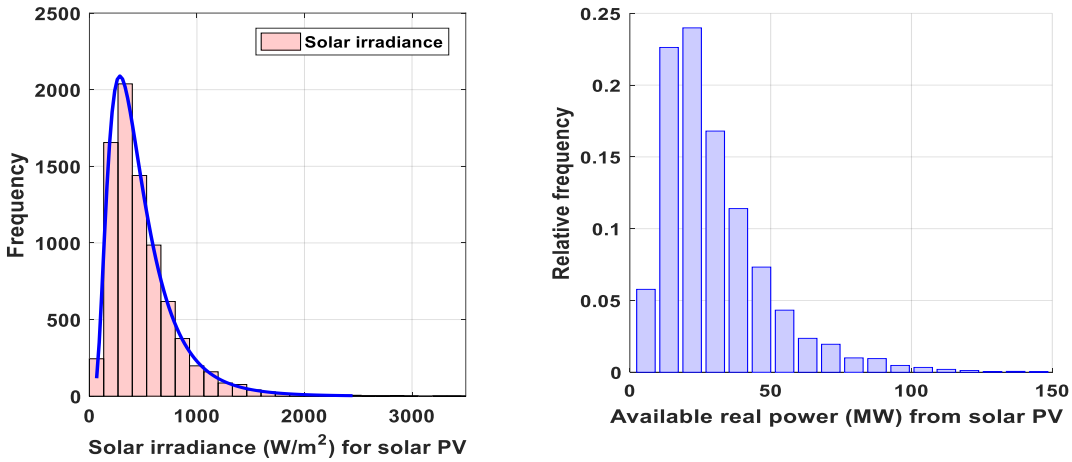


(a) Solar irradiance distribution (b) Active power distribution

**FIGURE 8.** **The distribution of solar irradiance and real power for the SPV units at bus 13.**

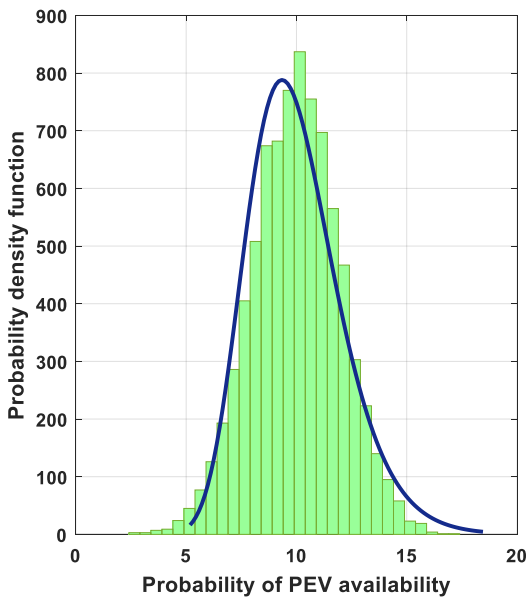


**FIGURE 9.** **The normal distribution for the EV unit at bus 11.**

Furthermore, Figure 9 shows the normal distribution for the EV unit which, in case studies 3 and 4, is located at bus 11 instead of the wind generator. 8000 Monte-Carlo simulations were performed in order to produce the power curve. For the EV unit located at bus 11, the parameters of the normal distribution are a mean of 10 and a standard deviation of 2.

In this case, the proposed MRGTO algorithm is applied to solve the OPF problem considering stochastic renewable energy sources (RES) with and without Vehicle-to-grid (V2G) technology, as below:

### 1) CASE 1: OPTIMIZATION OF THE FUEL COST WITH RES

The objective of the case study was to utilize the MRGTO algorithm to decrease the overall cost of power generation, while also confirming that the system constraints remained within their predetermined boundaries. The coefficients of the direct cost for WPGs were $g_{W_{d1}}$ = 1.6 and $g_{W_{d2}}$ = 1.75, and

the penalty cost coefficients for underutilized wind power were assumed to be $p_{W1}$= $p_{W2}$= 1.5, while the reserve cost coefficients for overestimation were $R_{W1}$= $R_{W2}$= 3. Also, the direct cost coefficient $g_{S_d}$, penalty cost coefficient $p_S$, and reserve cost coefficient $R_S$ for SPGs were proposed to be 1.6, 1.5, and 3, respectively. The best outcomes for cases 1 and 2 as produced by several algorithms, such as MRGTO, GTO, and MRFO, are shown in Table V. The results of the simulation clearly show that the suggested MRGTO method outperforms the other algorithms, achieving a minimum total cost of 781.5325 ($/h) for the first case.

Figure 10 illustrates the convergence behavior of the analyzed for the first Case using the studied algorithms. The convergence refers to the tendency of a system to approach a stable state or a consistent result over iterations. This stability is crucial as it indicates the reliability and effectiveness of the techniques being employed. The convergence behavior depicted in Figure 10 provides valuable insights into how quickly or slowly each technique reaches a stable solution, as well as any oscillations or fluctuations that may occur during the convergence process. From this figure, the convergence characteristics of the proposed MRGTO algorithm is faster than the conventional GTO and MRFO algorithms. This distinction underscores the efficacy and efficiency of the MRGTO technique in reaching a stable solution within fewer iterations, demonstrating its potential to significantly enhance computational efficiency and optimization performance in the analyzed context.

As seen in Figure 11a, all of the buses' voltage profiles for Case 1 were within the designated ranges. The generating unit's reactive power is a dependent or state variable in the OPF problem, and after optimization, the reactive power restrictions need to be met. Table V illustrates how the MRGTO algorithm effectively produces generator reactive powers within the specified bounds. Figure 12a displays the generator reactive power profile of all compared algorithms for case 1. A statistical study of several methods is displayed in Table VI such as EESWHO [48], WHO [48], MPA [15], MPSO [15], GA [15], GOA [49], BWOA [49], GWO [49], ALO [49], PSO [49], GSA [49], MFO [49], BMO [49], SHADE-SF [40], JS [50], CGO [50], FPA [50], GPC [50], WSO [51], NGO [51], POA [51], ESMA [52], SMA [52], BWOA [52], MSA [52], PSO [53], GA [53], TFWO [53], TLBO [53], TLTFWO [53], and MTFWO [54] in addition to the MRFO, GTO, and MRGTO algorithms for the first case. The table clearly shows that, in this particular example, the MRGTO algorithm outperforms both the traditional MRFO and GTO algorithms as well as the previously published methods.

Higher accuracy and robustness are delivered by the suggested MRGTO technique, as demonstrated by the results shown in Table VI. Additionally, the table validates MRGTO's efficacy and shows how it outperforms more than thirty well-known algorithms for the OPF problem. Boxplots are used to confirm that the method is effective in locating solutions inside a limited range. The shape of the boxplots demonstrates that the MRGTO algorithm regularly provides good outcomes and exhibits highly competitive performance relative to other approaches. The boxplots for case 1 in Fig. 13a indicate that the suggested MRGTO technique produces more precise optimization results. The boxplots' tight distribution suggests that the method can reliably find solutions inside a limited range, which is an important feature for handling issues of this nature.

TABLE V
THE OUTCOMES OF CASES 1 AND 2 FOR THE MRGTO ALGORITHM AND OTHER RECENTLY EMPLOYED OPTIMIZATION ALGORITHMS.

| | Min | Max | Case 1 | | | Case 2 | | |
|---|---|---|---|---|---|---|---|---|
| | | | **MRGTO** | **GTO** | **MRFO** | **MRGTO** | **GTO** | **MRFO** |
| Generator active power | | | | | | | | |
| $P_{G1}$(MW) | 50 | 200 | 134.9079 | 134.9079 | 134.9103 | 125.3276 | 125.1087 | 124.7534 |
| $P_{G2}$(MW) | 20 | 80 | 29.38132 | 26.76084 | 28.71013 | 33.09102 | 32.45242 | 31.47858 |
| $P_{W1}$(MW) | 0 | 75 | 44.27896 | 42.70002 | 43.28014 | 46.05411 | 45.70349 | 45.25554 |
| $P_{G8}$(MW) | 10 | 35 | 10.00017 | 10 | 10.00453 | 10 | 10 | 10.0002 |
| $P_{W2}$(MW) | 0 | 60 | 37.33276 | 35.99119 | 37.29648 | 38.79667 | 38.50471 | 38.12388 |
| $P_{S1}$(MW) | 0 | 50 | 33.26212 | 38.85147 | 34.98677 | 35.47765 | 36.97566 | 39.13389 |
| Generator voltage | | | | | | | | |
| $V_1$(p.u.) | 0.95 | 1.1 | 1.071628 | 1.072738 | 1.072514 | 1.070406 | 1.069948 | 1.070045 |
| $V_2$(p.u.) | 0.95 | 1.1 | 1.056928 | 1.057066 | 1.056861 | 1.056714 | 1.05631 | 1.056455 |
| $V_5$ (p.u.) | 0.95 | 1.1 | 1.034543 | 1.033222 | 1.034633 | 1.035572 | 1.035308 | 1.035155 |
| $V_8$ (p.u.) | 0.95 | 1.1 | 1.090462 | 1.06822 | 1.045422 | 1.064734 | 1.039887 | 1.092908 |
| $V_{11}$ (p.u.) | 0.95 | 1.1 | 1.099794 | 1.096972 | 1.096998 | 1.09835 | 1.099664 | 1.098441 |
| $V_{13}$ (p.u.) | 0.95 | 1.1 | 1.050028 | 1.043226 | 1.045881 | 1.049993 | 1.064558 | 1.049578 |
| Objective function | | | | | | | | |
| Fuel cost ($/h) | | | **781.5325** | 782.0754 | 781.9462 | 790.6934 | 791.3568 | 791.3423 |
| Fuel thermal unit cost | | | 443.5091 | 434.8298 | 441.2941 | 433.8454 | 431.1451 | 426.9973 |
| Wind generation cost | | | 249.4191 | 239.3955 | 245.8239 | 260.8168 | 258.5331 | 255.6042 |
| Solar generation cost | | | 88.60423 | 107.8501 | 94.82825 | 96.03116 | 101.6786 | 108.7408 |
| Emission (ton/h) | | | 1.761871 | 1.762517 | 1.762288 | 0.989614 | 0.977172 | 0.957355 |
| Total cost ($/h) | | | - | - | - | **808.3382** | 808.7798 | 808.4119 |
| Carbon tax ($/h) | | | - | - | - | 17.83 | 17.83 | 17.83 |
| Transmission loss (MW) | | | 5.763185 | 5.811409 | 5.78833 | 5.347085 | 5.345029 | 5.345496 |
| Voltage deviation (p.u.) | | | 0.456662 | 0.443573 | 0.447871 | 0.458937 | 0.499965 | 0.457548 |
| Generator reactive power | | | | | | | | |
| $Q_{G1}$(MVAR) | -20 | 150 | -2.80206 | -0.34855 | -0.48751 | -2.92847 | -3.28612 | -3.24456 |

| | | | | | | | | |
|---|---|---|---|---|---|---|---|---|
| $Q_{G2}$(MVAR) | -20 | 60 | 12.41104 | 12.91998 | 11.05175 | 11.08102 | 11.33861 | 11.5107 |
| $Q_{W1}$(MVAR) | -30 | 35 | 21.88723 | 21.35411 | 22.54309 | 22.25324 | 22.84209 | 22.28209 |
| $Q_{G8}$(MVAR) | -15 | 40 | 40 | 40 | 40 | 40 | 34.06228 | 40 |
| $Q_{W2}$(MVAR) | -25 | 30 | 30 | 30 | 29.88348 | 30 | 30 | 30 |
| $Q_{S1}$(MVAR) | -20 | 25 | 15.49823 | 13.23168 | 14.12589 | 15.44846 | 20.91078 | 15.32024 |

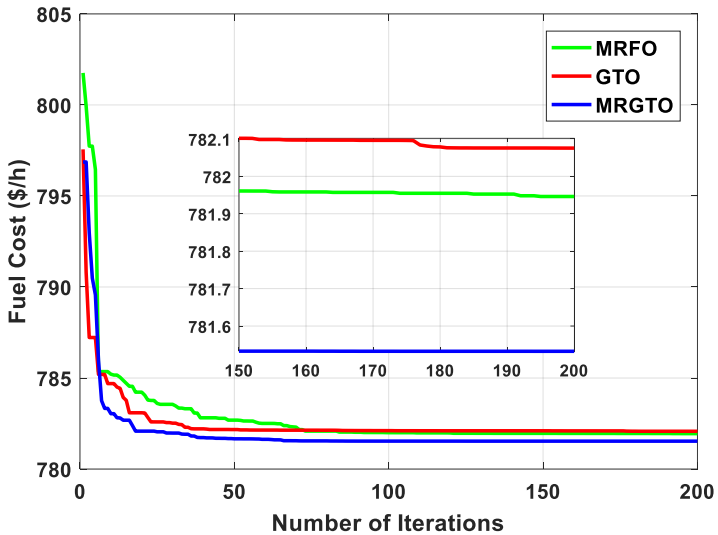


**FIGURE 10.** **The convergence behavior of the analyzed algorithms for Case 1.**

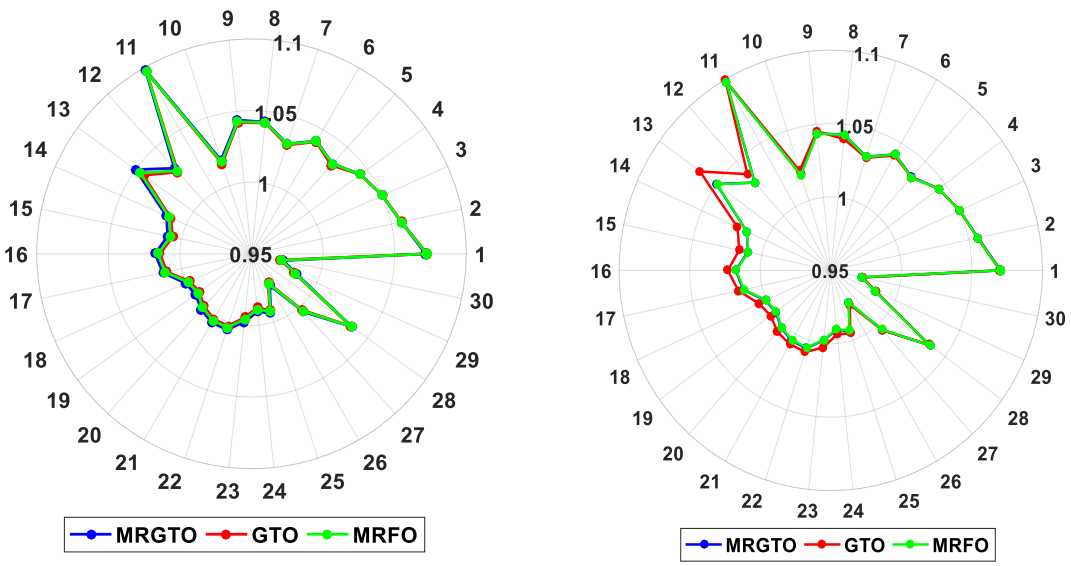


(a) Case 1 (b) Case 2

**FIGURE 11.** **The voltage magnitude of the examined techniques.**

This article has been accepted for publication in IEEE Access. This is the author's version which has not been fully edited and content may change prior to final publication. Citation information: DOI 10.1109/ACCESS.2024.3425754



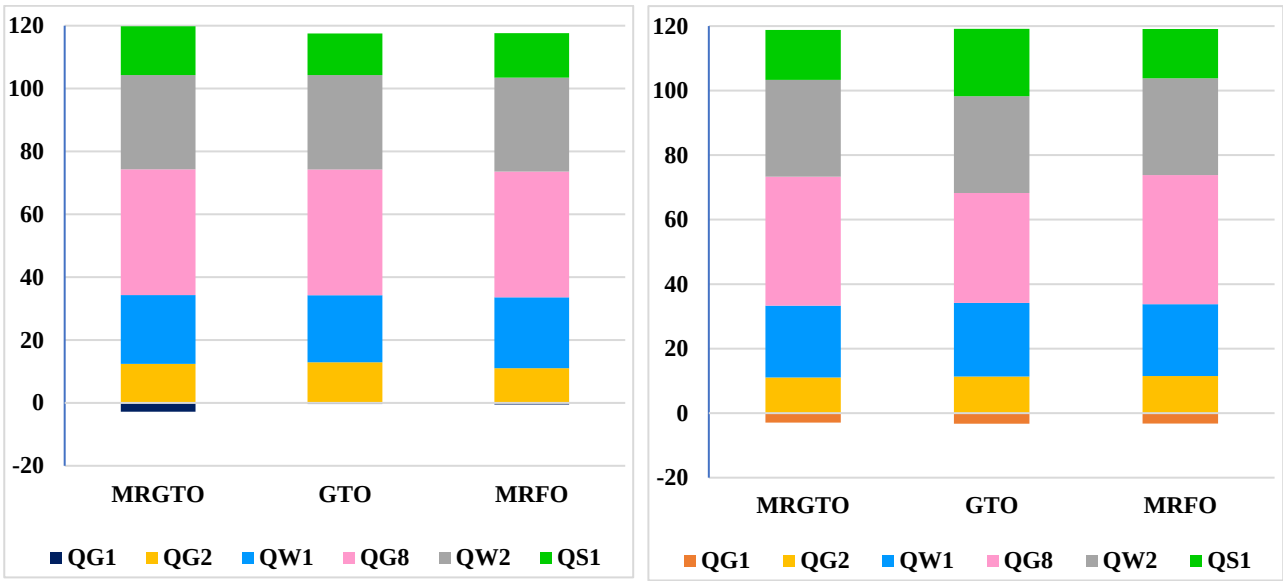


(a) Case 1 (b) Case 2

**FIGURE 12. The generator reactive power profile for all the algorithms.**

TABLE VI
THE STATISTICAL ANALYSIS CONDUCTED FOR THE FIRST CASE.

| Technique | Min. | Average | Median | Max. | STD |
|---|---|---|---|---|---|
| MRGTO | 781.5325 | 781.9982 | 781.898 | 782.4832 | 0.340527 |
| GTO | 782.0754 | 782.6609 | 782.5239 | 783.8048 | 0.594211 |
| MRFO | 781.9462 | 782.2266 | 782.261 | 782.4978 | 0.172706 |
| WHO [48] | 781.6866 | 782.1924 | 782.2067 | 782.7441 | 0.332675 |
| EESWHO [48] | 781.6322 | 782.3088 | 782.3227 | 782.8886 | 0.375421 |
| MPA [15] | 781.924 | 782.3531 | - | 782.6771 | 0.2474 |
| MPSO [15] | 782.9268 | 783.9104 | - | 786.06 | 0.9685 |
| GA [15] | 782.8023 | 783.1872 | - | 784.2214 | 0.3809 |
| GOA [49] | 785.7109 | 804.0168 | - | 823.4731 | 9.52 |
| BWOA [49] | 784.8148 | 788.2471 | - | 795.4683 | 5.83 |
| GWO [49] | 781.6645 | 783.0412 | - | 783.3359 | **0.275** |
| ALO [49] | 781.6562 | 784.3253 | - | 791.9234 | 2.49 |
| PSO [49] | 781.9047 | 784.9048 | - | 794.4221 | 2.52 |
| GSA [49] | 782.2237 | 785.8603 | - | 794.8996 | 2.43 |
| MFO [49] | 781.6928 | 782.492 | - | 783.9305 | 0.477 |
| BMO [49] | 781.6519 | 781.8187 | - | 783.5284 | 0.344 |
| SHADE-SF [40] | 782.30 | - | - | - | - |
| JS [50] | 781.6387 | - | - | - | - |
| CGO [50] | 782.195 | - | - | - | - |
| FPA [50] | 782.8596 | - | - | - | - |
| GPC [50] | 782.4229 | - | - | - | - |
| WSO [51] | 781.733 | 782.4562 | - | 783.7659 | 0.6722 |
| NGO [51] | 781.8438 | 782.335 | - | 782.9944 | 0.3766 |
| POA [51] | 782.1865 | 782.8452 | - | 785.3441 | 0.9205 |
| ESMA [52] | 781.9376 | - | - | - | - |
| SMA [52] | 781.958 | - | - | - | - |
| BWOA [52] | 784.342 | - | - | - | - |
| MSA [52] | 782.423 | - | - | - | - |
| PSO [53] | 782.71 | 783.2148 | - | 783.7969 | 0.89 |
| GA [53] | 783.2565 | 784.6206 | - | 786.7536 | 1.37 |
| TFWO [53] | 782.3068 | 782.6754 | - | 783.2645 | 0.63 |
| TLBO [53] | 782.4558 | 782.9740 | - | 783.8231 | 0.94 |
| TLTFWO [53] | 781.9791 | 782.2216 | - | 782.4136 | 0.20 |
| MTFWO [54] | 781.8715 | 781.9661 | - | 782.2456 | 0.25 |

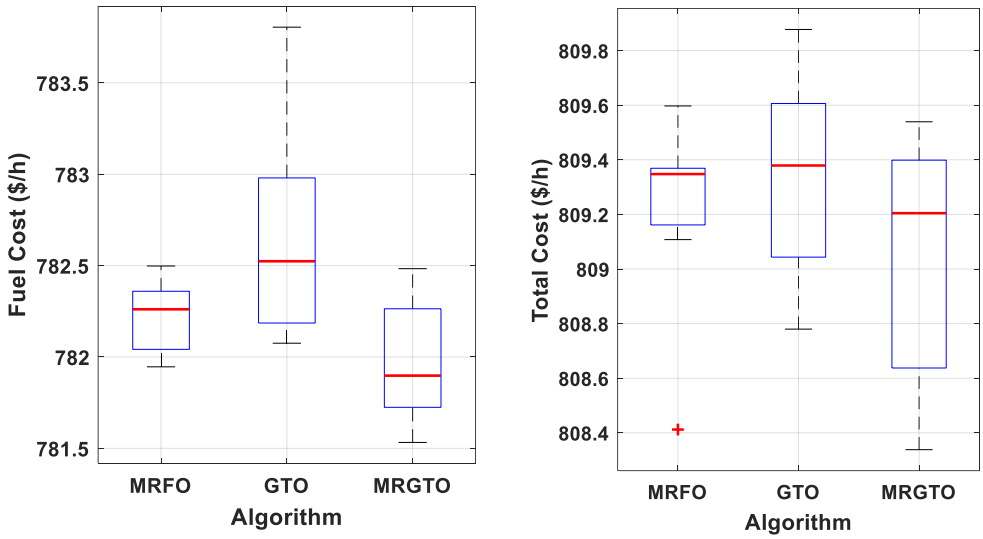


(a) Case 1 (b) Case 2

**FIGURE 13.** **The boxplots for all the compared algorithms for Cases 1 and 2.**

### 2) CASE 2: OPTIMIZATION OF THE FUEL COST WITH RES AND A CARBON TAX.

This section presents the analysis of the MRGTO technique's performance on the modified IEEE 30-bus test system, specifically in Case 2. The overall costs in this instance comprised the costs of thermal fuel, wind, photovoltaic, and emissions. As it was a single-objective minimization issue, the value of the fitness function corresponding to the total costs. The results of the MRGTO algorithm and other optimization techniques, such as MRFO and GTO, are displayed in Table V, where MRGTO achieves the lowest cost of 808.3382 $/h. Figure 14 shows the convergence curve for the algorithms under study, and Figure 12b shows the reactive powers for the generator bus that the algorithms produced. All calculated values are within the designated limits. The voltage profile for the load buses acquired from all the algorithms is combined in Figure 11b.

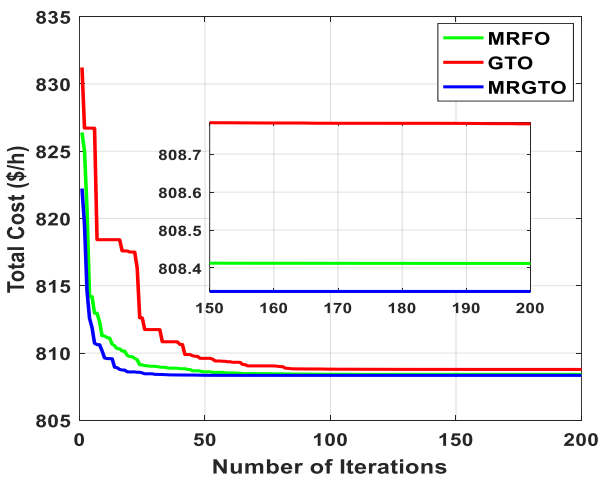


**FIGURE 14.** **The convergence behavior of the analyzed techniques for Case 2.**

The results of 20 runs of each method are shown in Table VII, together with the average simulation duration and the best, average, and worst output values for each objective function. In comparison to the GTO and MRFO algorithms, the suggested MRGTO method showed higher optimization and efficiency. The reliability of the MRGTO technique is evident from its outputs, which consistently outperformed those of other optimization methods, such as GBES [19], BES [19], DE [19], GOA [49], BWOA [49], GWO [49], ALO [49], PSO [49], GSA [49], MFO [49], BMO [49], GWO [55], SHADE-SF [40], ABC [55], CSA [55], JS [50], CGO [50], FPA [50], GPC [50], ESMA [52], SMA [52], BWOA [52], MSA [52], PSO [53], GA [53], TFWO [53], TLBO [53], TLTFWO [53], MTFWO [54]. Additionally, as shown in Figure 13b, boxplots were employed to assess the consistency of the optimal solutions obtained by the suggested MRGTO and other current algorithms.

TABLE VII
STATISTICAL ANALYSIS OF CASE STUDY 2.

| lgorithm | Min. | Mean | Median | Max. | STD |
|---|---|---|---|---|---|
| MRGTO | 808.3382 | 809.0565 | 809.2046 | 809.5393 | 0.399472 |
| GTO | 808.7798 | 809.3398 | 809.3791 | 809.8774 | 0.379161 |
| MRFO | 808.412 | 809.2303 | 809.3477 | 809.5973 | 0.317642 |
| GBES [19] | 808.7192 | 809.0436 | 809.0949 | 809.133 | 0.125 |
| BES [19] | 808.8582 | 809.6389 | 809.8551 | 810.1221 | 0.479 |
| DE [19] | 822.5771 | 834.8417 | 835.641 | 845.5061 | 7.461 |
| GOA [49] | 822.3074 | 839.1499 | - | 857.8005 | 9.32 |
| BWOA [49] | 821.4095 | 824.358 | - | 830.89 | 2.66 |
| GWO [49] | 811.2516 | 811.4707 | - | 811.6266 | 0.126 |
| ALO [49] | 811.4334 | 811.7083 | - | 814.2972 | 0.536 |
| PSO [49] | 811.5916 | 812.7758 | - | 818.8017 | 1.43 |
| GSA [49] | 811.5264 | 811.7708 | - | 813.3572 | 0.4.97 |
| MFO [49] | 811.4229 | 811.7398 | - | 812.4613 | 0.342 |
| BMO [49] | 810.7982 | 810.7739 | - | 811.1199 | 0.145 |
| GWO [55] | 809.93 | - | - | - | - |
| SHADE-SF [40] | 810.346 | - | - | - | - |
| ABC [55] | 811.26 | - | - | - | - |
| CSA [55] | 811.53 | - | - | - | - |
| JS [50] | 810.1201 | - | - | - | - |
| CGO [50] | 811.4568 | - | - | - | - |
| FPA [50] | 811.6664 | - | - | - | - |
| GPC [50] | 810.324 | - | - | - | - |
| ESMA [52] | 810.3558 | - | - | - | - |
| SMA [52] | 810.3739 | - | - | - | - |
| BWOA [52] | 812.0366 | - | - | - | - |
| MSA [52] | 810.8843 | - | - | - | - |
| PSO [53] | 811.4062 | 812.5325 | - | 813.5510 | 0.57 |
| GA [53] | 812.6163 | 813.7541 | - | 815.4792 | 2.25 |
| TFWO [53] | 811.3949 | 812.3127 | - | 813.1720 | 1.16 |
| TLBO [53] | 811.5219 | 812.3812 | - | 813.2546 | 1.43 |
| TLTFWO [53] | 810.8444 | 810.9632 | - | 811.2148 | 0.18 |
| MTFWO [54] | 810.2265 | 810.3940 | - | 810.4835 | 0.12 |

### 3) CASE 3: OPTIMIZATION OF THE FUEL COST WITH STOCHASTIC VEHICLE-TO-GRID AND RES

Table VIII presents the optimal solutions, as produced by the MRGTO algorithm and other algorithms covered in this article, for all conceivable configurations of the modified IEEE 30-bus power system, which now includes the EV generators in addition to the thermal, wind, and PV generators. The decision variable values demonstrate that all problem constraints are satisfied, proving the efficacy of the methods. The table also shows the lowest generation costs, or 790.5985, 790.7433, and 790.7578 $/h, that the corresponding generation schedules utilizing the MRGTO, MRFO, and GTO algorithms were able to achieve.

For the identical condition, the suggested MRGTO algorithm consistently finds the best solution, as do the MRFO and GTO algorithms. The convergence curves for these algorithms are displayed in Figure 15, where the suggested MRGTO performs better at convergence than the original MRFO and GTO methods. the reactive powers for the generator bus using the techniques are displayed in Figure 16a, and every value were within the given bounds. In OPF problems, the load bus's voltage profile is a crucial factor that needs to be carefully taken into account. Additionally, all buses' operating voltages must be between 0.95 and 1.1 p.u. Figure 17a presents a visual representation of the voltage profiles for Case 3, demonstrating that the optimization process has met the specified requirements successfully.

TABLE VIII
THE RESULTS OBTAINED FOR CASE 3, COMPARING THE PERFORMANCE OF THE MRGTO ALGORITHM TO THAT OF RECENT OPTIMIZATION ALGORITHMS.

| | **Min** | **Max** | **Case 3** | | | **Case 4** | | |
|---|---|---|---|---|---|---|---|---|
| | | | **MRGTO** | **GTO** | **MRFO** | **MRGTO** | **GTO** | **MRFO** |
| Generator active power | | | | | | | | |
| $P_{G1}$(MW) | 50 | 200 | 134.9079 | 134.9147 | 134.9102 | 128.71 | 128.931 | 128.7286 |
| $P_{G2}$(MW) | 20 | 80 | 42.65446 | 42.88033 | 44.13195 | 46.53888 | 47.8019 | 46.80258 |
| $P_{W1}$(MW) | 0 | 75 | 48.17972 | 47.61746 | 47.8695 | 48.90774 | 49.40477 | 48.96339 |
| $P_{G8}$(MW) | 10 | 35 | 10.00023 | 10.00166 | 10.00263 | 10 | 10 | 10.00339 |
| $P_{W2}$(MW) | 0 | 60 | 11.81638 | 11.83559 | 11.93693 | 11.92402 | 11.99354 | 11.94876 |
| $P_{S1}$(MW) | 0 | 50 | 42.15619 | 42.48824 | 40.89682 | 43.41195 | 41.37493 | 43.04765 |
| Generator voltage | | | | | | | | |
| $V_1$(p.u.) | 0.95 | 1.1 | 1.073781 | 1.072283 | 1.073093 | 1.072819 | 1.072221 | 1.072739 |
| $V_2$(p.u.) | 0.95 | 1.1 | 1.059454 | 1.058812 | 1.058692 | 1.059307 | 1.058872 | 1.058995 |

| | | | | | | | | |
|---|---|---|---|---|---|---|---|---|
| $V_5$ (p.u.) | 0.95 | 1.1 | 1.037196 | 1.037395 | 1.035647 | 1.037319 | 1.037559 | 1.036696 |
| $V_8$ (p.u.) | 0.95 | 1.1 | 1.038062 | 1.039324 | 1.087031 | 1.038244 | 1.063071 | 1.038203 |
| $V_{11}$ (p.u.) | 0.95 | 1.1 | 1.1 | 1.099438 | 1.098344 | 1.1 | 1.1 | 1.099933 |
| $V_{13}$ (p.u.) | 0.95 | 1.1 | 1.057408 | 1.060869 | 1.05367 | 1.059793 | 1.052084 | 1.062201 |
| Objective function | | | | | | | | |
| Fuel cost ($/h) | | | **790.5985** | 790.7433 | 790.7578 | 798.4438 | 798.2806 | 798.5125 |
| Fuel thermal unit cost | | | 490.0207 | 490.8738 | 495.4342 | 489.8514 | 495.0526 | 490.8848 |
| Wind generation cost | | | 155.5145 | 153.3653 | 154.3269 | 158.3181 | 160.2455 | 158.5334 |
| Solar generation cost | | | 119.8176 | 121.1857 | 115.2908 | 124.6182 | 117.0578 | 123.3429 |
| PEV generation cost | | | 25.24571 | 25.31847 | 25.70583 | 25.65617 | 25.92474 | 25.75143 |
| Emission (ton/h) | | | 1.759981 | 1.76071 | 1.760163 | 1.20728 | 1.223358 | 1.208619 |
| Total cost ($/h) | | | - | - | - | **819.9696** | 820.0931 | 820.0622 |
| Carbon tax ($/h) | | | - | - | - | 17.83 | 17.83 | 17.83 |
| Transmission loss (MW) | | | 6.314878 | 6.338008 | 6.348032 | 6.092641 | 6.106188 | 6.094371 |
| Voltage deviation (p.u.) | | | 0.458911 | 0.469984 | 0.451495 | 0.465705 | 0.452886 | 0.472146 |
| Generator reactive power | | | | | | | | |
| $Q_{G1}$(MVAR) | -20 | 150 | -1.84214 | -4.38956 | -2.12345 | -2.32171 | -3.03954 | -1.93687 |
| $Q_{G2}$(MVAR) | -20 | 60 | 13.81378 | 13.61564 | 12.11212 | 13.14153 | 11.3716 | 12.44868 |
| $Q_{W1}$(MVAR) | -30 | 35 | 23.02463 | 23.42983 | 21.39729 | 22.86799 | 22.4968 | 22.3947 |
| $Q_{G8}$(MVAR) | -15 | 40 | 34.16205 | 35.9093 | 40 | 34.06459 | 40 | 34.08843 |
| $Q_{PEV}$(MVAR) | -25 | 30 | 29.96487 | 29.41258 | 29.26405 | 29.80935 | 29.81514 | 29.66683 |
| $Q_{S1}$(MVAR) | -20 | 25 | 18.12346 | 19.30042 | 16.6371 | 18.97823 | 15.89177 | 19.87592 |

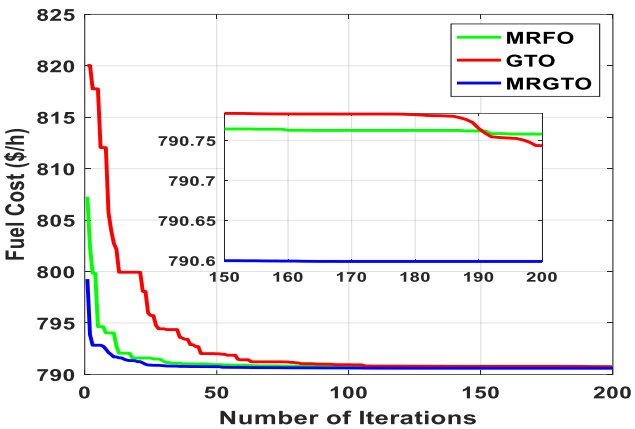


**FIGURE 15.** **The convergence behavior of the analyzed techniques for Cases 3 and 4.**

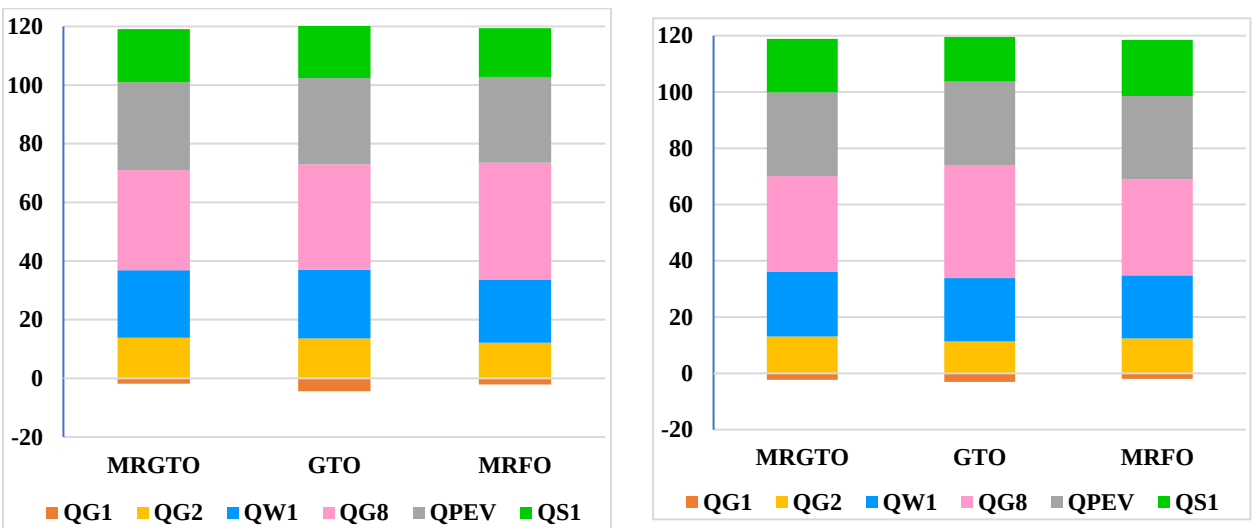


(a) Case 3 (b) Case 4

**FIGURE 16.** **The generator reactive power profile of the studied techniques.**

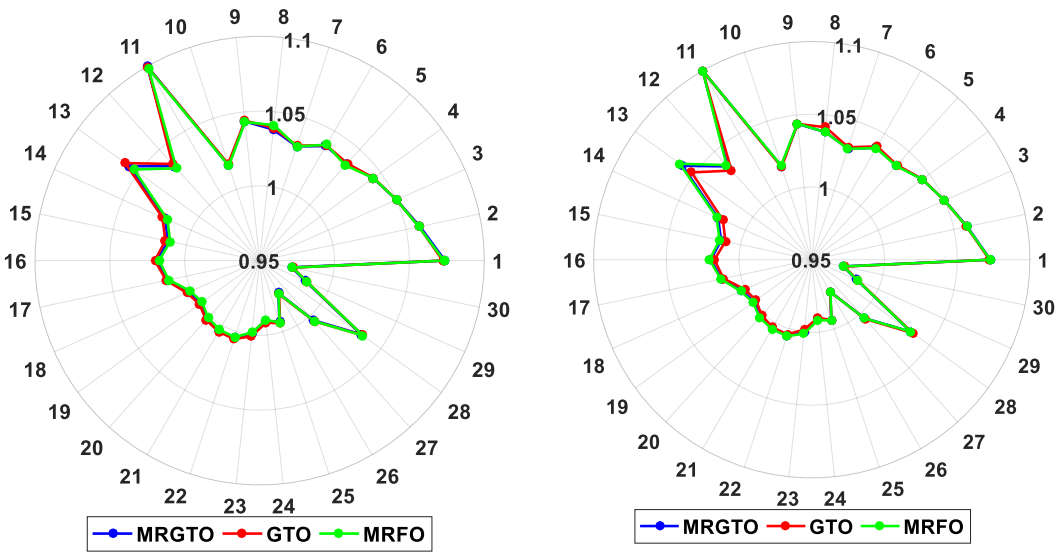


(a) Case 3 (b) Case 4

**FIGURE 17.** **The voltage magnitude of the studied techniques for Cases 3 and 4.**

Table IX presents the standard deviation values for the best and average results obtained by the MRGTO algorithm and other algorithms considered in this study. The low standard deviation values obtained by MRGTO for both best and average results suggest that it achieved an optimal or near-optimal solution during each run. Figure 18a presents a boxplot that visually compares the distribution results of all algorithms over 20 runs in this case. The plot demonstrates that MRGTO exhibit strong and consistent performance, with showing higher accuracy than other algorithms.

TABLE IX
STATISTICAL ANALYSIS OF CASE STUDY 3.

| Algorithm | Min. | Mean | Median | Max. | STD |
|---|---|---|---|---|---|
| MRGTO | 790.5985 | 791.0494 | 791.0774 | 791.4633 | 0.346048 |
| GTO | 790.7433 | 791.2288 | 791.2592 | 791.6889 | 0.336478 |
| MRFO | 790.7578 | 791.2036 | 791.2509 | 791.5453 | 0.245773 |
| GBES [19] | 791.3507 | 791.8828 | 791.8873 | 792.4156 | 0.294026 |
| BES [19] | 791.4415 | 792.2648 | 792.2981 | 793.1239 | 0.416398 |
| DE [19] | 802.5099 | 830.6065 | 828.8514 | 854.9425 | 21.55934 |
| LSO [19] | 807.1078 | 823.5439 | 823.6603 | 850.6178 | 14.8507 |
| SMA [19] | 804.8356 | 822.0662 | 819.609 | 840.6084 | 10.68986 |

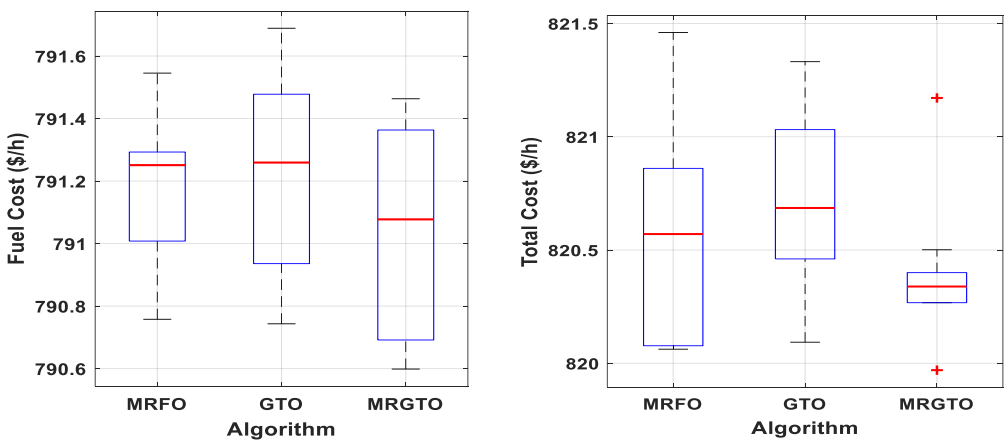


(a) Case 3 (b) Case 4

**FIGURE 18.** **Boxplots comparing the performance of the studied methods for the third and fourth Cases.**

#### 4) CASE 4: OPTIMIZATION OF THE OPERATING COST WITH A CARBON TAX AND STOCHASTIC VEHICLE-TO-GRID AND RES.

In this scenario, the aim was to minimize the total cost of thermal, wind, PV, and PEV generation as well as the emission cost. The proposed MRGTO algorithm and other well-known methods were employed to achieve this objective. The optimal solutions and control variable values for these methods are presented in Tables VIII. Additionally, Figure 19 illustrates that the MRGTO algorithm demonstrates a better convergence rate than the original GTO and MRFO methods. These findings indicate the superiority of the MRGTO algorithm over existing methods in terms of optimality and convergence. The generator reactive power profile of all compared algorithms for Case 4 is shown in Figure 16b. Furthermore, Figure 17b displays the voltage profiles of the MRGTO, GTO, and MRFO algorithms for the whole buses.

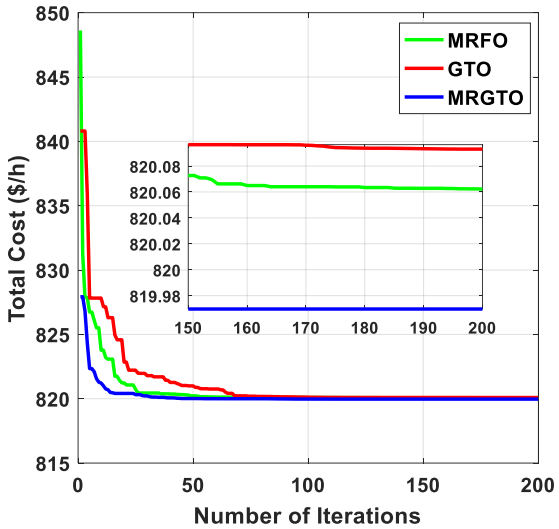


**FIGURE 19. The convergence behavior of the analyzed techniques for Case 4.**

Table X showcases that the MRGTO algorithm achieved low standard deviation values for both the best and average outcomes, indicating that it likely reached an optimal or nearly optimal solution during the simulation. Figure 18b presents a visual representation of the consistency of the proposed MRGTO and other existing algorithms in achieving the optimal solution, using boxplots.

TABLE X
STATISTICAL ANALYSIS OF CASE STUDY 4.

| Algorithm | Min. | Mean | Median | Max. | STD |
|---|---|---|---|---|---|
| MRGTO | **819.9696** | **820.3886** | **820.3388** | **821.1714** | **0.307322** |
| GTO | 820.0931 | 820.7106 | 820.6857 | 821.3316 | 0.400932 |
| MRFO | 820.0622 | 820.5963 | 820.5705 | 821.4605 | 0.465448 |
| GBES [19] | 820.373 | 821.016 | 820.9745 | 821.5573 | 0.341034 |
| BES [19] | 820.4051 | 821.0891 | 821.0207 | 821.9714 | 0.516716 |
| DE [19] | 825.7615 | 837.9958 | 838.0892 | 847.4443 | 6.939199 |
| LSO [19] | 833.2156 | 843.8339 | 842.8787 | 859.0379 | 9.426536 |
| SMA [19] | 831.9909 | 840.2487 | 840.0777 | 848.1718 | 5.895258 |

#### 5) CASE 5: STOCHASTIC DYNAMIC OPTIMAL POWER FLOW CONSIDERING THE VEHICLE-TO-GRID AND RES

The stochastic OPF with variation of load demand was suggested in the comprehensive information. Table XI provides a comprehensive overview of 24 representative scenarios. Each scenario is uniquely identified by a scenario number, and the ratio loading of Pd. As shown in Table XI, the lowest share of power from the wind Turbines, PV, and EV occurs when the system load is at its least level (scenario 3, with a loading of 39.27834%). Minimum loading corresponds to the lowest existing in the grid, resulting in lower transmission losses. Conversely, the highest share of power from the wind Turbines, PV, and EV is recorded while the system is operating at its maximum load (scenario 1, with a loading of 104.0753%).

TABLE XI
COMPREHENSIVE OVERVIEW OF 24 REPRESENTATIVE SCENARIOS.

| Scenario number | % Loading *Pd* | Wind power (MW) | PV power (MW) | EV power (MW) |
|---|---|---|---|---|
| 1 | 104.0753 | 75 | 49.99999 | 10.84417 |
| 2 | 97.48467 | 75 | 50 | 10.17107 |
| 3 | 39.27834 | 0 | 23.57336 | 9.042482 |
| 4 | 101.5853 | 75 | 50 | 15 |
| 5 | 99.74474 | 75 | 50 | 10.10425 |
| 6 | 81.36331 | 75 | 50 | 10.92151 |
| 7 | 49.23189 | 2.247454 | 50 | 9.107048 |
| 8 | 58.27154 | 27.68968 | 49.98975 | 9.257913 |
| 9 | 92.444 | 74.99933 | 49.99985 | 10.3593 |
| 10 | 86.17302 | 75 | 49.99999 | 10.73568 |
| 11 | 44.91196 | 1.082235 | 38.95371 | 8.951662 |
| 12 | 94.30378 | 75 | 50 | 10.29915 |
| 13 | 79.54886 | 75 | 50 | 15 |
| 14 | 61.78872 | 37.65572 | 49.99763 | 9.130649 |
| 15 | 76.77018 | 74.99957 | 50 | 10.91434 |
| 16 | 65.08182 | 46.81012 | 50 | 9.344616 |
| 17 | 51.47053 | 8.292616 | 49.99324 | 9.336999 |
| 18 | 68.83229 | 57.43867 | 49.99796 | 9.355709 |
| 19 | 71.53372 | 65.73984 | 49.90447 | 9.643435 |
| 20 | 83.21835 | 75 | 50 | 15 |
| 21 | 74.18913 | 72.96787 | 49.87712 | 9.276738 |
| 22 | 89.64533 | 75 | 50 | 10.53808 |
| 23 | 54.48136 | 16.8702 | 49.98561 | 9.286423 |
| 24 | 42.01018 | 0 | 31.30776 | 9.265005 |

Figure 20 illustrates the ratio loading of Pd (demand) obtained through Monte Carlo simulations in Case 5. The data presented in Figure 20 provides insights into how the system's load demand varies under different scenarios and conditions. By analyzing the ratio loading of Pd, one can understand the system's resilience, its ability to handle fluctuations, and its overall operational performance. This figure serves as a valuable tool for decision-makers and researchers in assessing the reliability and efficiency of the electric power system, especially in scenarios involving high penetration of renewable energy sources and electric vehicles.

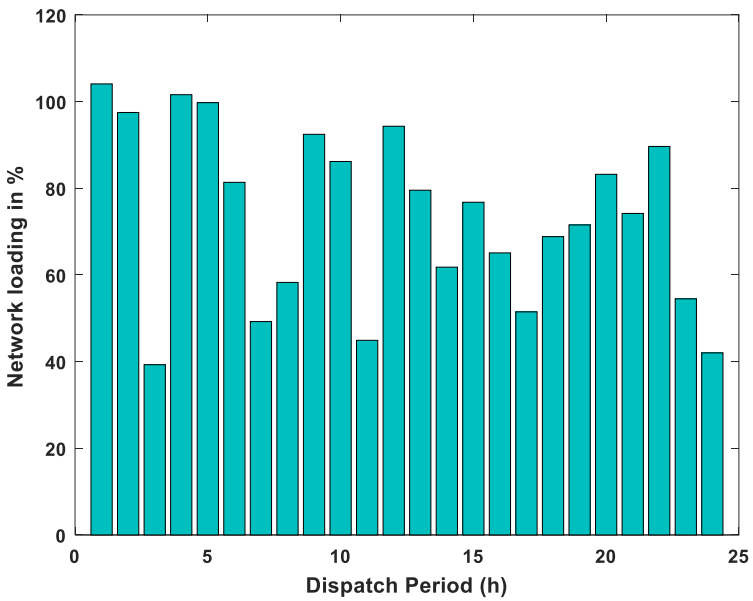


**FIGURE 20. The ratio loading of Pd through Monte Carlo simulations (Case 5).**

Table XII presents the outcomes derived from Case 5 utilizing the proposed MRGTO algorithm. Each scenario is detailed with respective values for various parameters. These parameters include PG1, PG2, and PG8 representing thermal power generation outputs from different sources, Pw1 indicating wind power generation, and Ps1 denoting solar power generation. Additionally, PPEV refers to the power supplied by plug-in electric vehicles (PEVs). The table also lists fuel costs, emissions, power loss, and voltage deviation, providing comprehensive insights into the algorithm's

performance under different conditions. These results serve as valuable data for evaluating the efficacy and competence of the MRGTO algorithm in optimizing power flow and resource allocation within the electric power system. It is noted from this table that the lowest value of the fuel cost (objective function) is when the system load is at its least level (scenario 3) and in the opposite while the system load is the highest level, the fuel cost has the most value (646.5487 $/h).

TABLE XII
THE RESULTS OBTAINED FOR CASE 5 USING THE PROPOSED MRGTO ALGORITHM.

| Scenario no. | $P_{G1}$ | $P_{G2}$ | $P_{w1}$ | $P_{G8}$ | $P_{s1}$ | $P_{PEV}$ | Fuel cost ($/h) | Emission (ton/h) | Power loss (MW) | Voltage deviation (p.u.) |
|---|---|---|---|---|---|---|---|---|---|---|
| 1 | 134.9076 | 20.00318 | 75 | 10 | 49.99999 | 10.84417 | 646.5487 | 1.76454 | 5.805432 | 0.484136 |
| 2 | 115.7349 | 20 | 75 | 10 | 50 | 10.17107 | 600.0138 | 0.581431 | 4.634414 | 0.520734 |
| 3 | 50.12255 | 20 | 0 | 10.00034 | 23.57336 | 9.042482 | 240.5447 | 0.104086 | 1.423994 | 0.332423 |
| 4 | 123.0207 | 20 | 75 | 10 | 50 | 15 | 636.0603 | 0.869355 | 5.128004 | 0.476559 |
| 5 | 122.6258 | 20 | 75 | 10 | 50 | 10.10425 | 615.9663 | 0.84999 | 5.053485 | 0.487961 |
| 6 | 65.95518 | 21.0508 | 75 | 10.00012 | 50 | 10.92151 | 470.1903 | 0.117454 | 2.343977 | 0.601591 |
| 7 | 49.99935 | 20 | 2.247454 | 10 | 50 | 9.107048 | 286.485 | 0.104028 | 1.830691 | 0.681217 |
| 8 | 49.99808 | 20 | 27.68968 | 10 | 49.98975 | 9.257913 | 331.2372 | 0.104027 | 1.793868 | 0.341524 |
| 9 | 100.485 | 20 | 74.99933 | 10 | 49.99985 | 10.3593 | 563.1211 | 0.282061 | 3.857219 | 0.463935 |
| 10 | 81.40477 | 20 | 75 | 10 | 49.99999 | 10.73568 | 512.3199 | 0.153266 | 2.926082 | 0.566418 |
| 11 | 49.97538 | 20 | 1.082235 | 10.00175 | 38.95371 | 8.951662 | 266.5029 | 0.104016 | 1.684241 | 0.214687 |
| 12 | 106.06 | 20 | 75 | 10 | 50 | 10.29915 | 576.9872 | 0.359535 | 4.102292 | 0.520387 |
| 13 | 55.9813 | 21.4697 | 75 | 10 | 50 | 15 | 457.7996 | 0.107071 | 2.009524 | 0.614698 |
| 14 | 49.99979 | 20 | 37.65572 | 10.00025 | 49.99763 | 9.130649 | 348.4848 | 0.104028 | 1.674812 | 0.726302 |
| 15 | 53.56624 | 20 | 74.99957 | 10 | 50 | 10.91434 | 428.952 | 0.105949 | 1.913468 | 0.639959 |
| 16 | 49.98313 | 20 | 46.81012 | 10.00016 | 50 | 9.344616 | 364.8399 | 0.10402 | 1.696134 | 0.438499 |
| 17 | 49.99917 | 20 | 8.292616 | 10 | 49.99324 | 9.336999 | 297.4368 | 0.104028 | 1.754539 | 0.774314 |
| 18 | 50.00033 | 20 | 57.43867 | 10 | 49.99796 | 9.355709 | 383.4855 | 0.104028 | 1.721966 | 0.447705 |
| 19 | 49.42911 | 20.00132 | 65.73984 | 10 | 49.90447 | 9.643435 | 397.4399 | 0.103767 | 1.991612 | 0.61549 |
| 20 | 68.24005 | 20 | 75 | 10 | 50 | 15 | 490.7913 | 0.121206 | 2.39926 | 0.595829 |
| 21 | 49.9929 | 20 | 72.96787 | 10.00009 | 49.87712 | 9.276738 | 410.3174 | 0.104025 | 1.862729 | 0.331108 |
| 22 | 91.91248 | 20 | 75 | 10 | 50 | 10.53808 | 541.0691 | 0.20543 | 3.395703 | 0.547323 |
| 23 | 50.00003 | 20 | 16.8702 | 10 | 49.98561 | 9.286423 | 312.3486 | 0.104028 | 1.742098 | 0.764619 |
| 24 | 50.01649 | 20.0003 | 0 | 10 | 31.30776 | 9.265005 | 252.9555 | 0.104036 | 1.532709 | 0.233594 |

Figure 21 illustrates the hourly power share of Thermal, Wind Turbine (WT), Photovoltaic (PV), and Plug-in Electric Vehicles (PEV) obtained through the implementation of the MRGTO algorithm in the fifth Case. This figure provides a visual representation of how power generation from different sources varies throughout the day.

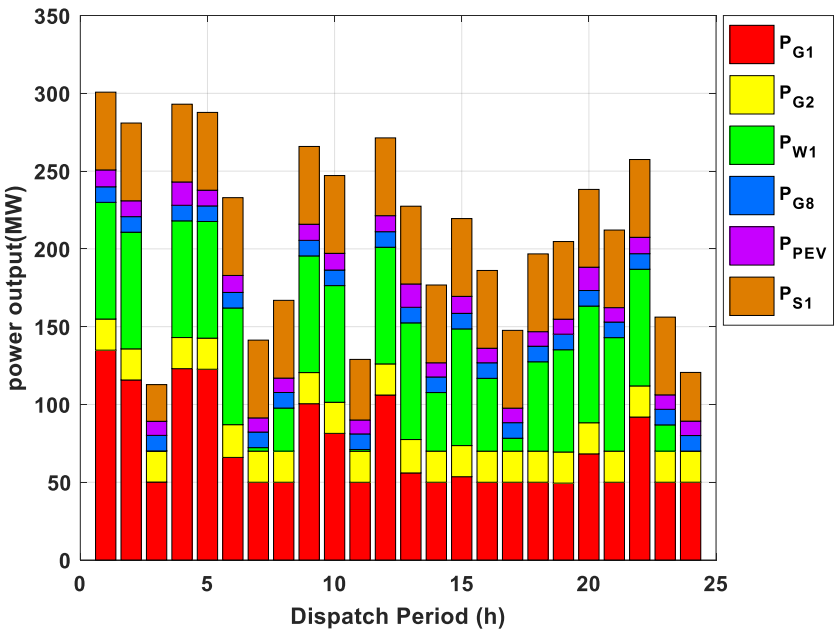


**FIGURE 21. Hourly active power share of Thermal, WT, PV, and PEV using MRGTO algorithm (Case 5).**

Figure 22 displays the voltage profile for each scenario for the case 5. Figure 24 presents the best settings of the decision variables for the respective scenarios in the fifth Case. It is clear that the voltages are within their permissible bounds. The reactive power settings of the units for these scenarios in this case are displayed in Figures 23.

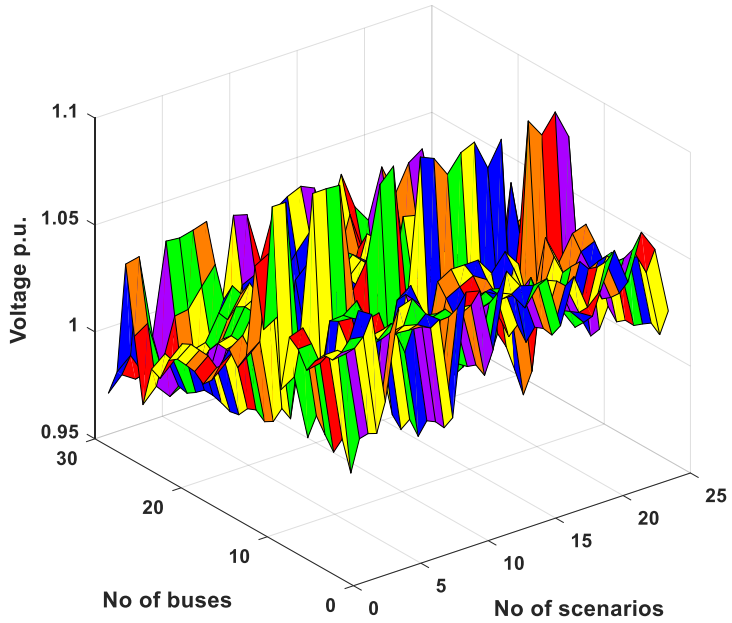


**FIGURE 22.** **Voltage profiles of the load bus in the scenarios of Case 5.**

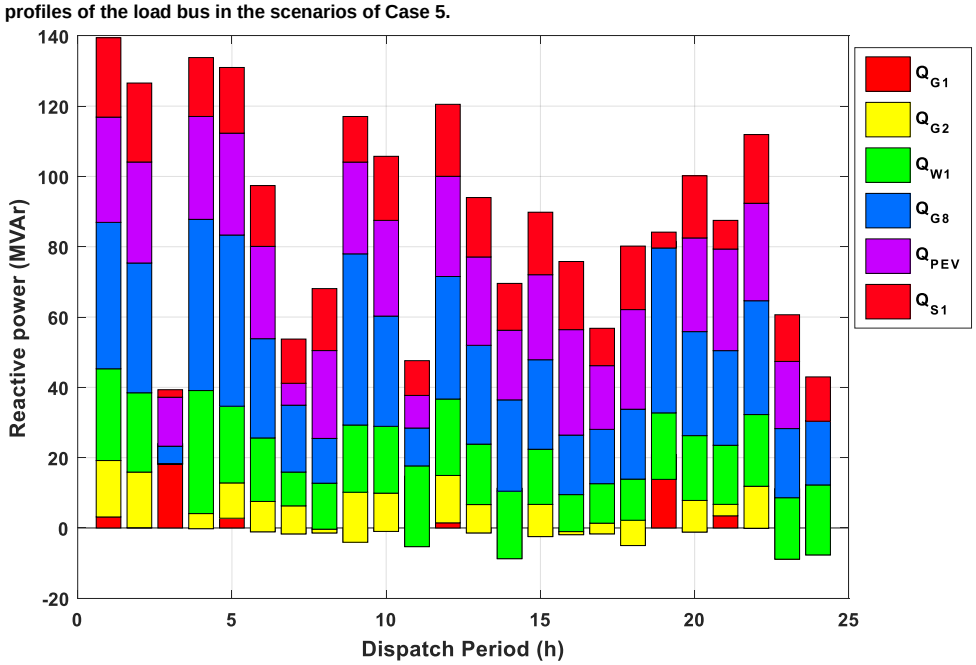


**FIGURE 23.** **The reactive power settings of the generation units for every scenario in the fifth Case.**

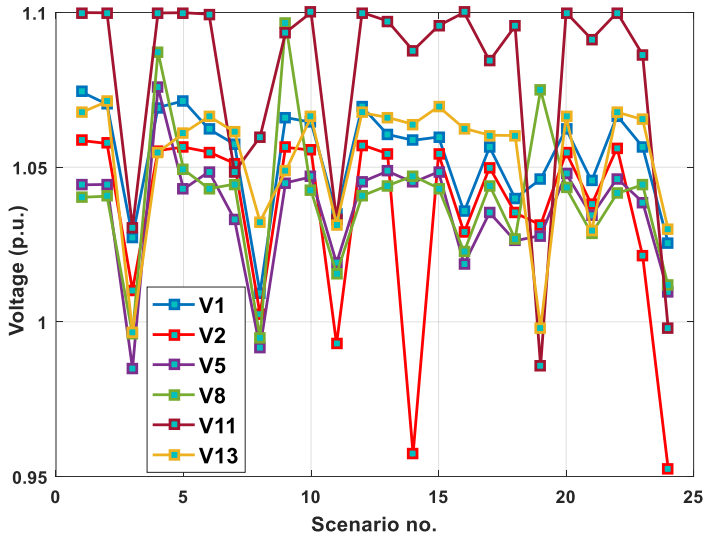


**FIGURE 24.** **The best PV bus voltage values for the scenarios within Case 5.**

Figure 25 depicts the hourly generation cost of Thermal, Wind Turbine (WT), Photovoltaic (PV), and Plug-in Electric Vehicles (PEV) across different scenarios utilizing the MRGTO algorithm in Case 5. This visualization provides a detailed breakdown of the costs of power generation from various sources over a day. Thermal generation typically involves higher costs due to fuel expenses and operational considerations than renewable sources like WT and PV, which benefit from free fuel sources (wind and sunlight). By analyzing the hourly generation costs for each scenario and energy source, stakeholders can evaluate the economic implications of different power generation strategies and assess the feasibility of participating renewable energy and electric vehicles into the system. This figure is a valuable tool for decision-makers in optimizing generation strategies to minimize costs while ensuring reliability and sustainability in the electric power system.

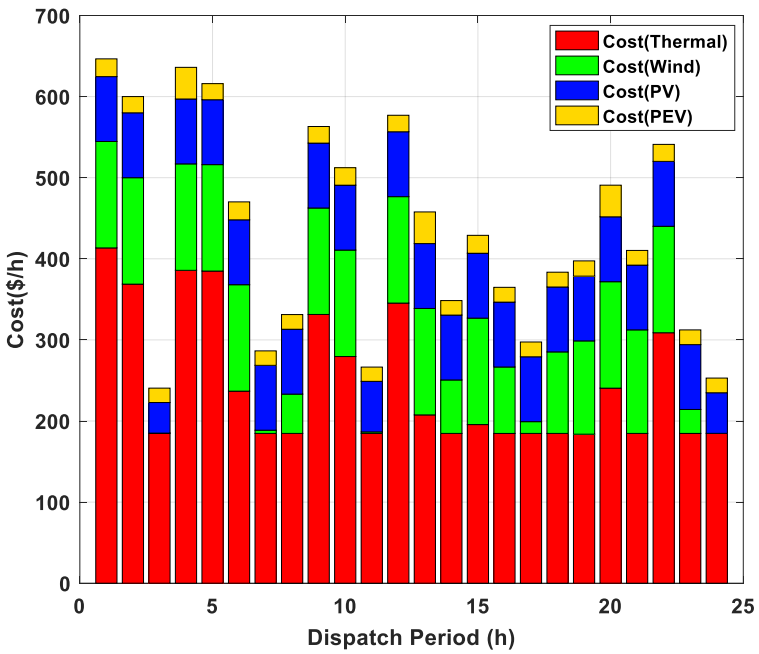


**FIGURE 25.** **Hourly generation cost of Thermal, WT, PV, and PEV units for each scenarios using MRGTO algorithm (Case 5).**

## VI. Conclusions

in this paper, to improve the more complicated optimal power flow (OPF) problem, the novel hybrid metaheuristic optimization algorithm (MRGTO) has been created and presented. The MRGTO algorithm was used to regulate the DOPF solutions for an IEEE 30-bus system with traditional thermal generators and wind turbine, photovoltaic (PV), and

plug-in electric vehicle (PEV) units in order to assess its efficacy. First, the proposed algorithm was evaluated by applying it to seven numerical optimization test functions. Based on benchmark statistical data, it was found that the MRGTO outperformed seven popular optimization techniques, including MRFO, BWO, RUN, DBO, TSO, and the original GTO algorithm. Furthermore, the MRGTO algorithm effectively reduced both emissions and the overall system generating costs from the stochastic OPF problem. Four cases were examined in order to demonstrate the efficacy of the suggested MRGTO approach. In the first two scenarios, the focus was on defining the optimum control settings for the IEEE 30-bus system without PEVs. These scenarios included adding wind and PV beside the two thermal power plants. In comparison to other methods, the acquired findings show that the MRGTO method performs better.

The proposed MRGTO produced outstanding results, obtaining the lowest hourly fuel cost of $781.5325 per hour for the first case and the lowest hourly total cost of $808.3382 per hour. These results provide strong proof of the MRGTO's superiority over other contemporary techniques in terms of control variable optimization. In the third and fourth scenarios, renewable energy resources like wind, photovoltaics, and PEVs were employed to simulate the OPF problem, and the best control variables were determined using the suggested MRGTO technique. The MRGTO achieved the lowest fitness values of $790.5985 per hour and $819.9696 per hour, demonstrating impressive consistency outperformance. In comparison to the other algorithms under study, the MRGTO algorithm demonstrated a quick and steady convergence characteristic curve and outperformed algorithms like MRFO and GTO algorithms. Additionally, the suggested MRGTO algorithm is assessed through comparison with various heuristic approaches documented in the recent literature. In Case 5, The MRGTO algorithm's exploration effectiveness remained consistent across iterations, avoiding local optima solutions. In Case 5, the MRGTO algorithm successfully optimized power generation from Thermal, Wind Turbine (WT), Photovoltaic (PV), and PEVs, as evidenced by the hourly power share and generation cost analyses. The obtained results showcase the algorithm's effectiveness in managing power generation from diverse sources, optimizing generation costs, and accommodating the variability inherent in renewable energy and electric vehicle integration. Overall, the MRGTO algorithm in Case 5 provides valuable insights into the optimization of power flow in complex systems, highlighting its potential for enhancing sustainability, efficiency, and reliability in the electric power grid. The MRGTO algorithm may eventually be used for planning and expansion studies related to power systems, such as those involving the addition of hydropower, fuel cell, and hydrogen power generation.

## REFERENCES

[1] D. Çelik, M. E. Meral, and M. Waseem, "Investigation and analysis of effective approaches, opportunities, bottlenecks and future potential capabilities for digitalization of energy systems and sustainable development goals," *Electric Power Systems Research*, vol. 211, p. 108251, Oct. 2022, doi: 10.1016/j.epsr.2022.108251.

[2] A. Alzahrani, S. K. Ramu, G. Devarajan, I. Vairavasundaram, and S. Vairavasundaram, "A Review on Hydrogen-Based Hybrid Microgrid System: Topologies for Hydrogen Energy Storage, Integration, and Energy Management with Solar and Wind Energy," *Energies (Basel)*, vol. 15, no. 21, p. 7979, Oct. 2022, doi: 10.3390/en15217979.

[3] J. A. Momoh and S. Surender Reddy, "Review of optimization techniques for Renewable Energy Resources," in *2014 IEEE Symposium on Power Electronics and Machines for Wind and Water Applications*, IEEE, Jul. 2014, pp. 1–8. doi: 10.1109/PEMWA.2014.6912225.

[4] S. S. Reddy and P. R. Bijwe, "Real time economic dispatch considering renewable energy resources," *Renew Energy*, vol. 83, pp. 1215–1226, Nov. 2015, doi: 10.1016/j.renene.2015.06.011.

[5] R. Roy and H. T. Jadhav, "Optimal power flow solution of power system incorporating stochastic wind power using Gbest guided artificial bee colony algorithm," *International Journal of Electrical Power & Energy Systems*, vol. 64, pp. 562–578, Jan. 2015, doi: 10.1016/j.ijepes.2014.07.010.

[6] P. P. Biswas, P. N. Suganthan, R. Mallipeddi, and G. A. J. Amaratunga, "Optimal reactive power dispatch with uncertainties in load demand and renewable energy sources adopting scenario-based approach," *Appl Soft Comput*, vol. 75, pp. 616–632, Feb. 2019, doi: 10.1016/j.asoc.2018.11.042.

[7] L. T. Al-Bahrani, B. Horan, M. Seyedmahmoudian, and A. Stojcevski, "Dynamic economic emission dispatch with load dema nd management for the load demand of electric vehicles during crest shaving and valley filling in smart cities environment," *Energy*, vol. 195, p. 116946, Mar. 2020, doi: 10.1016/j.energy.2020.116946.

[8] S. S. Reddy, "Optimal scheduling of thermal-wind-solar power system with storage," *Renew Energy*, vol. 101, pp. 1357–1368, Feb. 2017, doi: 10.1016/j.renene.2016.10.022.

[9] S. Surender Reddy, P. R. Bijwe, and A. R. Abhyankar, "Real-Time Economic Dispatch Considering Renewable Power Generation Variability and Uncertainty Over Scheduling Period," *IEEE Syst J*, vol. 9, no. 4, pp. 1440–1451, Dec. 2015, doi: 10.1109/JSYST.2014.2325967.

[10] T. N. Bhattarai, S. Ghimire, B. Mainali, S. Gorjian, H. Treichel, and S. R. Paudel, "Applications of smart grid technology in Nepal: status, challenges, and opportunities," *Environmental Science and Pollution Research*, vol. 30, no. 10, pp. 25452–25476, Feb. 2022, doi: 10.1007/s11356-022-19084-3.

[11] M. A. M. Shaheen *et al.*, "Enhanced transient search optimization algorithm-based optimal reactive power dispatch including electric vehicles," *Energy*, vol. 277, p. 127711, Aug. 2023, doi: 10.1016/j.energy.2023.127711.

[12] S. R. Salkuti, "Emerging and Advanced Green Energy Technologies for Sustainable and Resilient Future Grid," *Energies (Basel)*, vol. 15, no. 18, p. 6667, Sep. 2022, doi: 10.3390/en15186667.

[13] M. H. Hassan, S. K. Elsayed, S. Kamel, C. Rahmann, and I. B. M. Taha, "Developing chaotic Bonobo optimizer for optimal power flow analysis considering stochastic renewable energy resources," *Int J Energy Res*, vol. 46, no. 8, pp. 11291–11325, Jun. 2022, doi: 10.1002/er.7928.

[14] S. S. Reddy, V. Sandeep, and C.-M. Jung, "Review of stochastic optimization methods for smart grid," *Frontiers in Energy*, vol. 11, no. 2, pp. 197–209, Jun. 2017, doi: 10.1007/s11708-017-0457-7.

[15] M. Farhat, S. Kamel, A. M. Atallah, and B. Khan, "Developing a Marine Predator Algorithm for Optimal Power Flow Analysis considering Uncertainty of Renewable Energy Sources," *International Transactions on Electrical Energy Systems*, vol. 2022, pp. 1–16, Jun. 2022, doi: 10.1155/2022/3714475.

[16] J. Sarda, K. Pandya, and K. Y. Lee, "Dynamic optimal power flow with cross entropy covariance matrix adaption evolutionary strategy for systems with electric vehicles and renewable generators," *Int J Energy Res*, vol. 45, no. 7, pp. 10869–10881, Jun. 2021, doi: 10.1002/er.6571.

[17] P. P. Biswas, P. N. Suganthan, B. Y. Qu, and G. A. J. Amaratunga, "Multiobjective economic-environmental power dispatch with stochastic wind-solar-small hydro power," *Energy*, vol. 150, pp. 1039–1057, May 2018, doi: 10.1016/j.energy.2018.03.002.

[18] M. Ghasemi, P. Trojovský, E. Trojovská, and M. Zare, "Gaussian bare-bones Levy circulatory system-based optimization for power flow in the presence of renewable units," *Engineering Science and Technology, an International Journal*, vol. 47, p. 101551, Nov. 2023, doi: 10.1016/j.jestch.2023.101551.

[19] M. H. Hassan, S. Kamel, J. L. Domínguez-García, and R. J. J. Molu, "Integrating renewable energy and V2G uncertainty into optimal power flow: A gradient bald eagle search optimization algorithm with local escaping operator," *IET Renewable Power Generation*, Nov. 2023, doi: 10.1049/rpg2.12874.

[20] Z. He, J. Zhou, N. Sun, B. Jia, and H. Qin, "Integrated scheduling of hydro, thermal and wind power with spinning reserve," *Energy Procedia*, vol. 158, pp. 6302–6308, Feb. 2019, doi: 10.1016/j.egypro.2019.01.409.

[21] A. Vaderobli, D. Parikh, and U. Diwekar, "Optimization under Uncertainty to Reduce the Cost of Energy for Parabolic Trough Solar Power Plants for Different Weather Conditions," *Energies (Basel)*, vol. 13, no. 12, p. 3131, Jun. 2020, doi: 10.3390/en13123131.

[22] M. Mohamed, A.-R. Youssef, M. Ebeed, and S. Kamel, "Hybrid Optimization Technique for Short Term Wind-Solar-Hydrothermal Generation Scheduling," in *2019 IEEE Conference on Power Electronics and Renewable Energy (CPERE)*, IEEE, Oct. 2019, pp. 212–216. doi: 10.1109/CPERE45374.2019.8980237.

[23] M. H. Hassan, S. K. Elsayed, S. Kamel, C. Rahmann, and I. B. M. Taha, "Developing chaotic Bonobo optimizer for optimal power flow analysis considering stochastic renewable energy resources," *Int J Energy Res*, vol. 46, no. 8, pp. 11291–11325, Jun. 2022, doi: 10.1002/er.7928.

[24] M. Farhat, S. Kamel, M. A. Elseify, and A. Y. Abdelaziz, "A modified white shark optimizer for optimal power flow considering uncertainty of renewable energy sources," *Sci Rep*, vol. 14, no. 1, p. 3051, Feb. 2024, doi: 10.1038/s41598-024-53249-z.

[25] M. J. Morshed, J. Ben Hmida, and A. Fekih, "A probabilistic multi-objective approach for power flow optimization in hybrid wind-PV-PEV systems," *Appl Energy*, vol. 211, pp. 1136–1149, Feb. 2018, doi: 10.1016/j.apenergy.2017.11.101.

[26] G. E. Alvarez, "Stochastic optimization considering the uncertainties in the electricity demand, natural gas infrastructures, photovoltaic units, and wind generation," *Comput Chem Eng*, vol. 160, p. 107712, Apr. 2022, doi: 10.1016/j.compchemeng.2022.107712.

[27] N. Alamir, S. Kamel, M. H. Hassan, and S. M. Abdelkader, "An improved weighted mean of vectors algorithm for microgrid energy management considering demand response," *Neural Comput Appl*, Jul. 2023, doi: 10.1007/s00521-023-08813-5.

[28] Y. Ma and Y. Bai, "A multi-population differential evolution with best-random mutation strategy for large-scale global optimization," *Applied Intelligence*, vol. 50, no. 5, pp. 1510–1526, May 2020, doi: 10.1007/s10489-019-01613-2.

[29] W. Ye, W. Feng, and S. Fan, "A novel multi-swarm particle swarm optimization with dynamic learning strategy," *Appl Soft Comput*, vol. 61, pp. 832–843, Dec. 2017, doi: 10.1016/j.asoc.2017.08.051.

[30] M. A. El-Dabah, M. H. Hassan, S. Kamel, M. A. Abido, and H. M. Zawbaa, "Optimal Tuning of Power System Stabilizers for a Multi-Machine Power Systems Using Hybrid Gorilla Troops and Gradient-Based Optimizers," *IEEE Access*, vol. 11, pp. 27168–27188, 2023, doi: 10.1109/ACCESS.2023.3250384.

[31] A. M. Shaheen, A. R. Ginidi, R. A. El-Sehiemy, A. El-Fergany, and A. M. Elsayed, "Optimal parameters extraction of photovoltaic triple diode model using an enhanced artificial gorilla troops optimizer," *Energy*, vol. 283, p. 129034, Nov. 2023, doi: 10.1016/j.energy.2023.129034.

[32] M. M. Elymany, M. A. Enany, and N. A. Elsonbaty, "Hybrid optimized-ANFIS based MPPT for hybrid microgrid using zebra optimization algorithm and artificial gorilla troops optimizer," *Energy Convers Manag*, vol. 299, p. 117809, Jan. 2024, doi: 10.1016/j.enconman.2023.117809.

[33] K. Nusair and F. Alasali, "Optimal Power Flow Management System for a Power Network with Stochastic Renewable Energy Resources Using Golden Ratio Optimization Method," *Energies (Basel)*, vol. 13, no. 14, p. 3671, Jul. 2020, doi: 10.3390/en13143671.

[34] P. P. Biswas, P. N. Suganthan, and G. A. J. Amaratunga, "Optimal power flow solutions incorporating stochastic wind and solar power," *Energy Convers Manag*, vol. 148, pp. 1194–1207, Sep. 2017, doi: 10.1016/j.enconman.2017.06.071.

[35] G. Ala *et al.*, "Different Scenarios of Electric Mobility: Current Situation and Possible Future Developments of Fuel Cell Vehicles in Italy," *Sustainability*, vol. 12, no. 2, p. 564, Jan. 2020, doi: 10.3390/su12020564.

[36] S. S. Reddy, "Optimization of Renewable Energy Resources in Hybrid Energy Systems," *Journal of Green Engineering*, vol. 7, no. 1, pp. 43–60, 2017, doi: 10.13052/jge1904-4720.7123.

[37] H. M. Dubey, M. Pandit, and B. K. Panigrahi, "Hybrid flower pollination algorithm with time-varying fuzzy selection mechanism for wind integrated multi-objective dynamic economic dispatch," *Renew Energy*, vol. 83, pp. 188–202, Nov. 2015, doi: 10.1016/j.renene.2015.04.034.

[38] F. Daqaq, M. H. Hassan, S. Kamel, and A. G. Hussien, "A leader supply-demand-based optimization for large scale optimal power flow problem considering renewable energy generations," *Sci Rep*, vol. 13, no. 1, p. 14591, Sep. 2023, doi: 10.1038/s41598-023-41608-1.

[39] S. S. Reddy and P. R. Bijwe, "Real time economic dispatch considering renewable energy resources," *Renew Energy*, vol. 83, pp. 1215–1226, Nov. 2015, doi: 10.1016/j.renene.2015.06.011.

[40] P. P. Biswas, P. N. Suganthan, and G. A. J. Amaratunga, "Optimal power flow solutions incorporating stochastic wind and solar power," *Energy Convers Manag*, vol. 148, pp. 1194–1207, Sep. 2017, doi: 10.1016/j.enconman.2017.06.071.

[41] R. K. Avvari and V. K. D M, "A new hybrid evolutionary algorithm for multi-objective optimal power flow in an integrated WE, PV, and PEV power system," *Electric Power Systems Research*, vol. 214, p. 108870, Jan. 2023, doi: 10.1016/j.epsr.2022.108870.

[42] B. Abdollahzadeh, F. Soleimanian Gharehchopogh, and S. Mirjalili, "Artificial gorilla troops optimizer: A new nature-inspired metaheuristic algorithm for global optimization problems," *International Journal of Intelligent Systems*, vol. 36, no. 10, pp. 5887–5958, Oct. 2021, doi: 10.1002/int.22535.

[43] W. Zhao, Z. Zhang, and L. Wang, "Manta ray foraging optimization: An effective bio-inspired optimizer for engineering applications," *Eng Appl Artif Intell*, vol. 87, p. 103300, Jan. 2020, doi: 10.1016/j.engappai.2019.103300.

[44] M. H. Hassan, E. H. Houssein, M. A. Mahdy, and S. Kamel, "An improved Manta ray foraging optimizer for cost-effective emission dispatch problems," *Eng Appl Artif Intell*, vol. 100, p. 104155, Apr. 2021, doi: 10.1016/j.engappai.2021.104155.

[45] M. H. Hassan, S. Kamel, A. Alateeq, A. Alassaf, and I. Alsaleh, "Optimal Power Flow Analysis With Renewable Energy Resource Uncertainty: A Hybrid AEO-CGO Approach," *IEEE Access*, vol. 11, pp. 122926–122961, 2023, doi: 10.1109/ACCESS.2023.3328958.

[46] S. Duman, S. Rivera, J. Li, and L. Wu, "Optimal power flow of power systems with controllable wind-photovoltaic energy systems via differential evolutionary particle swarm optimization," *International Transactions on Electrical Energy Systems*, vol. 30, no. 4, pp. 1–28, 2020, doi: 10.1002/2050-7038.12270.

[47] M. Riaz, A. Hanif, S. J. Hussain, M. I. Memon, M. U. Ali, and A. Zafar, "An Optimization-Based Strategy for Solving Optimal

Power Flow Problems in a Power System Integrated with Stochastic Solar and Wind Power Energy," *Applied Sciences*, vol. 11, no. 15, p. 6883, Jul. 2021, doi: 10.3390/app11156883.

[48] M. H. Hassan, S. Kamel, and A. G. Hussien, "Optimal power flow analysis considering renewable energy resources uncertainty based on an improved wild horse optimizer," *IET Generation, Transmission & Distribution*, Jun. 2023, doi: 10.1049/gtd2.12900.

[49] M. H. Sulaiman and Z. Mustaffa, "Optimal power flow incorporating stochastic wind and solar generation by metaheuristic optimizers," *Microsystem Technologies*, vol. 27, no. 9, pp. 3263–3277, Sep. 2021, doi: 10.1007/s00542-020-05046-7.

[50] M. Farhat, S. Kamel, A. M. Atallah, and B. Khan, "Optimal Power Flow Solution Based on Jellyfish Search Optimization Considering Uncertainty of Renewable Energy Sources," *IEEE Access*, vol. 9, pp. 100911–100933, 2021, doi: 10.1109/ACCESS.2021.3097006.

[51] M. A. Ali, S. Kamel, M. H. Hassan, E. M. Ahmed, and M. Alanazi, "Optimal Power Flow Solution of Power Systems with Renewable Energy Sources Using White Sharks Algorithm," *Sustainability*, vol. 14, no. 10, p. 6049, May 2022, doi: 10.3390/su14106049.

[52] M. Farhat, S. Kamel, A. M. Atallah, M. H. Hassan, and A. M. Agwa, "ESMA-OPF: Enhanced Slime Mould Algorithm for Solving Optimal Power Flow Problem," *Sustainability*, vol. 14, no. 4, p. 2305, Feb. 2022, doi: 10.3390/su14042305.

[53] M. Alanazi, A. Alanazi, A. Y. Abdelaziz, and P. Siano, "Power Flow Optimization by Integrating Novel Metaheuristic Algorithms and Adopting Renewables to Improve Power System Operation," *Applied Sciences*, vol. 13, no. 1, p. 527, Dec. 2022, doi: 10.3390/app13010527.

[54] A. S. Alghamdi, "Optimal Power Flow in Wind–Photovoltaic Energy Regulation Systems Using a Modified Turbulent Water Flow-Based Optimization," *Sustainability*, vol. 14, no. 24, p. 16444, Dec. 2022, doi: 10.3390/su142416444.

[55] I. U. Khan, N. Javaid, K. A. A. Gamage, C. J. Taylor, S. Baig, and X. Ma, "Heuristic Algorithm Based Optimal Power Flow Model Incorporating Stochastic Renewable Energy Sources," *IEEE Access*, vol. 8, pp. 148622–148643, 2020, doi: 10.1109/ACCESS.2020.3015473.

MOHAMED H. HASSAN received the B.Sc. degree (Hons.) in electrical engineering from Minia University, Egypt, in 2011, the M.Sc. degree in electrical engineering from Cairo University, Egypt, in 2018, and the joint Ph.D. degree supervision between Aswan University, Egypt, and University of Jaen, Spain, in 2022. He has published more than 60 papers in reputable journals and international conferences. His research interests include optimization techniques, power system analysis, renewable energy, and smart grids.

SALAH KAMEL received the international joint Ph.D. degree from Jaen University, Spain (Main), and Aalborg University, Denmark (Host), in January 2014. He is currently an Associate Professor with the Department of Electrical Engineering, Aswan University. He is also the Leader of the Advanced Power Systems Research Laboratory (APSR Lab), Power Systems Research Group, Aswan, Egypt. His research interests include power system analysis and optimization, smart grid, and renewable energy systems.

EHAB MAHMOUD MOHAMED (Member, IEEE) received the Ph.D. degree in information science and electrical engineering from Kyushu University, Japan, in 2012. He is currently a Full Professor with the Department of Electrical Engineering, College of Engineering in Wadi Addwasir, Prince Sattam bin Abdulaziz University, Saudi Arabia. He is also a Full Professor with the Department of Electrical Engineering, Aswan University, Egypt. He has been a Specially Appointed Researcher with Osaka University, Japan, from 2013 to 2016. He has more than 150 journals and conference papers. His current research interests include 5G/ 6G networks, cognitive radio networks, millimeter wave transmissions, Li-Fi technology, MIMO systems, and reconfigurable intelligent surfaces. He is a technical committee member of many international conferences and a reviewer of many international conferences, journals, and transactions, especially highly ranked IEEE TRANSACTIONS/journals. He was the General Chair of the IEEE ITEMS'16 and IEEE ISWC'18 and a guest editor in many highly ranked transactions/journals.

SID AHMED EL MEHDI ARDJOUN received the State Engineer, Magister, Science Doctorate, and H.D.R. degrees in electrical engineering (option: electrical control and electromechanical converters) from Djillali Liabes University, Algeria, in 2008, 2010, 2016, and 2019, respectively. Since 2010, he has been with the IRECOM Laboratory as a Researcher. Since 2013, he has been with the Faculty of Electrical Engineering as a Lecturer. His research interests include electric control (robust control, intelligent control, and fault tolerant control) in renewable energy and electric drives domain.